

DAMTP-2001-78
20 August, 2001

FORMATION OF TOPOLOGICAL DEFECTS IN GAUGE FIELD THEORIES

ARTTU RAJANTIE

*Department of Applied Mathematics and Theoretical Physics
University of Cambridge, Wilberforce Road
Cambridge CB3 0WA, United Kingdom*

When a symmetry gets spontaneously broken in a phase transition, topological defects are typically formed. The theoretical picture of how this happens in a breakdown of a global symmetry, the Kibble-Zurek mechanism, is well established and has been tested in various condensed matter experiments. However, from the viewpoint of particle physics and cosmology, gauge field theories are more relevant than global theories. In recent years, there have been significant advances in the theory of defect formation in gauge field theories, which make precise predictions possible, and in experimental techniques that can be used to test these predictions in superconductor experiments. This opens up the possibility of carrying out relatively simple and controlled experiments, in which the non-equilibrium phase transition dynamics of gauge field theories can be studied. This will have a significant impact on our understanding of phase transitions in the early universe and in heavy ion collider experiments. In this paper, I review the current status of the theory and the experiments in which it can be tested.

1. Introduction

The formation of topological defects in phase transitions is a very generic phenomenon in physics. It can be studied experimentally in different condensed matter systems, but it is also believed to have happened during the early evolution of the universe,^{1,2} and the produced topological defects may have observable consequences to the properties of the universe today. Defect formation also has many similarities with the non-equilibrium phenomena that take place in heavy ion collisions.^{3,4}

In this article, however, we discuss defect formation in field theories as a physical phenomenon in its own right, as a unique way of obtaining information about the non-equilibrium dynamics of field theories. Theoretical calculations of phase transition dynamics are only possible in practice if one is willing to make many simplifying approximations and assumptions, and it is not at all clear which of these are actually justified. In this respect, it is useful that quantum field theories are applicable very generally in physics. Very similar field theories describe a wide range of systems from superconductors to interactions of elementary particles. In particular, the problems faced in theoretical calculations are identical in these systems. This raises the hope of testing some theoretical predictions in condensed matter experiments,⁵ in order to find out which approximations are reliable and how one should treat the field theories of particle physics theoretically.

To a certain extent, this hope has already been realized in equilibrium field the-

2 *Formation of topological defects in gauge field theories*

ory. Critical phenomena can be studied experimentally in many condensed matter systems, and they form the basis for the non-perturbative picture of quantum field theories.⁶ In particular, the concept of renormalization group, which is based on the critical behaviour of field theories near second order transitions points, is crucial for our understanding of particle physics.

In the case of non-equilibrium dynamics, both experiments and theoretical calculations are significantly more difficult, and therefore less progress has been made. In particular, it is very difficult to study directly the non-equilibrium dynamics during a phase transition in any experiment. Topological defects play a special role in this respect, because they survive for a long time after the phase transition, when the system has otherwise equilibrated. Their number density and spatial distribution carry information about the dynamics of the phase transition, and they can be compared to predictions of theoretical calculations.

In many ways, this approach is very similar to particle cosmology, where we hope to extract some information about particle physics from the relics of the Big Bang, and to particle accelerator experiments, in which we cannot observe the collision itself, but by studying its products we can reconstruct it. The difference is that superconductors and other condensed matter systems are theoretically simpler to treat and experimentally they allow much more control of different parameters. Of course, they cannot give any direct information about particle physics, but they will, nonetheless, help us understand the non-equilibrium dynamics of gauge field theories and in particular how they can be studied theoretically.

Indeed, the need for reliable tools for studying non-equilibrium gauge field theories is now greater than ever before, as the Relativistic Heavy Ion Collider, which has already started operation, and the Large Hadron Collider, which is scheduled to start by 2005, will be able to study directly the quark-gluon plasma phase of quantum chromodynamics. The heavy-ion collisions in these experiments are so complicated that very reliable and accurate theoretical calculations are needed in order to confront the experimental results, but our present understanding of the theory is too rudimentary for that. The insight provided by condensed matter experiments is therefore likely to be extremely useful. In particular, it is believed that at a certain value of the beam energy, the quark-gluon plasma produced in the collision cools through a second-order transition point.⁷ The relevant dynamics can then be described as freezing out of long-wavelength modes,^{3,4} very much like in the theories of defect formation.

So far, the formation of topological defects has been studied in liquid crystal^{8,9} and superfluid experiments,^{10,11,12,13} which are systems with global symmetries. The theoretical scenario that is believed to be applicable in this case is the Kibble-Zurek mechanism,^{1,5} but the experiments have produced mixed results. From the viewpoint of particle physics and cosmology, theories with global symmetries are less interesting than gauge field theories, whose natural condensed matter realization is superconductivity. The dynamics of gauge field theories are more complicated, but a theory of defect formation has been developed recently¹⁴ for Abelian systems, such

as superconductors. At the same time, the rapid progress in experimental techniques in the recent years has made accurate superconductor experiments possible.

The purpose of this paper is to review the current theoretical status of defect formation in field theories, with a special emphasis on gauge field theories. The various applications of topological defects in other fields such as cosmology are outside the scope of this article, and have been discussed in other reviews.^{2,15,16}

Throughout this paper, we shall use natural units, *i.e.*, $c = \hbar = k_B = \mu_0 = 1$. The structure of this paper is the following: In Section 2, we discuss the classification and basic properties of topological defects in field theories. In Section 3, we present the basics of finite-temperature field theories and phase transitions. Defect formation in first-order phase transitions is discussed in Section 4. Second-order phase transitions are more complicated but also more relevant physically, and are discussed in Section 5. In Section 6, we present different approximations that have been used to study the dynamics of phase transitions theoretically, and in Section 7, we discuss different condensed matter experiments that have been carried out or proposed.

2. Topological defects

2.1. Spontaneous symmetry breakdown

In most field theories, the Lagrangian $\mathcal{L}[\phi]$ is invariant under certain transformations $\phi \rightarrow g(\phi)$, *i.e.*,

$$\mathcal{L}[g(\phi)] = \mathcal{L}[\phi], \quad (1)$$

where g is an element of the symmetry group G , typically a Lie group. The fields of the theory, which are here denoted by ϕ for simplicity, can be in any representation of the group, and this determines the action of the transformation g on the field configuration.

In particle physics, these symmetries are often *gauge* symmetries, which means that the group element g can be a function of space and time. For instance, the Lagrangian of quantum electrodynamics is

$$\mathcal{L} = -\frac{1}{4}F_{\mu\nu}F^{\mu\nu} + \bar{\psi}(i\gamma^\mu D_\mu - m)\psi, \quad (2)$$

where $D_\mu = \partial_\mu + ieA_\mu$ and $F_{\mu\nu} = \partial_\mu A_\nu - \partial_\nu A_\mu$ are the covariant derivative and the field strength tensor, respectively. This Lagrangian is invariant under $U(1)$ gauge transformations

$$\psi(x) \rightarrow \exp(i\alpha(x))\psi(x), \quad A_\mu(x) \rightarrow A_\mu(x) - e^{-1}\partial_\mu\alpha(x). \quad (3)$$

In the limit $e \rightarrow 0$, the gauge field A_μ decouples, and the Lagrangian is only invariant if α is constant in space. In this case, the symmetry is said to be *global*.

Gauge symmetries are extremely important in particle physics, because besides electromagnetism, weak and strong interactions are described by $SU(2)$ and $SU(3)$

gauge groups, respectively. Global symmetries, on the other hand, are more common in condensed matter physics.

There are situations in which a symmetry of the Lagrangian is not reflected by the state of the system, and the symmetry is said to be *spontaneously broken*. Let us, for instance, consider a model with a single complex scalar field

$$\mathcal{L} = \partial_\mu \phi^* \partial^\mu \phi - V(|\phi|). \quad (4)$$

This Lagrangian is invariant under global U(1) transformations $\phi \rightarrow \exp(i\alpha)\phi$, where α is a constant in space-time. In a classical field theory, the vacuum state is simply the one in which ϕ minimizes the potential V and is constant in space and time. If, for instance, the potential has the form

$$V(|\phi|) = m^2|\phi|^2 + \lambda|\phi|^4, \quad (5)$$

and $m^2 < 0$, there is a set of degenerate minima at $|\phi| = (-m^2/2\lambda)^{1/2} \equiv v$, and therefore the system has many vacua, which are related to each other by symmetry transformations. Small perturbations around any of these vacua do not possess the U(1) symmetry, which means that the symmetry is broken. In the presence of quantum or thermal fluctuations, the situation is more subtle, and we cannot say whether the symmetries are broken simply by looking at the shape of the potential. These cases are discussed in more detail in Section 3.

If the symmetry group G that is broken is more complicated than U(1), it may also be partially broken. This happens if the vacuum remains invariant under a subgroup H of G . Suppose, for instance, that the full symmetry group is SU(2), and it is broken by an adjoint scalar field $\Phi = \sum_i \Phi^i \sigma^i$, where σ^i are the Pauli matrices. Under symmetry transformations, Φ transforms as $\Phi \rightarrow g^\dagger \Phi g$, where g is an SU(2) matrix. Because all vacuum states are equivalent, we can assume $\Phi = \Phi^3 \sigma^3$. Then Φ is invariant under transformations $g = \exp(i\alpha \sigma^3)$, which form a U(1) subgroup of the full SU(2) symmetry group.

2.2. Classification of defects

Let us now consider static classical solutions when a symmetry is spontaneously broken. To be a solution, a field configuration must approach the vacuum asymptotically at infinity. However, instead of a unique vacuum, the system has a set \mathcal{M} of vacua, which is called the vacuum manifold. In the above examples of U(1) and SU(2) symmetries, \mathcal{M} is topologically a circle and a sphere, respectively.

It is possible to have field configurations in which ϕ approaches a different point in \mathcal{M} in different directions. In this case, the values of ϕ at spatial infinity form a mapping $\phi : S^{D-1} \rightarrow \mathcal{M}$, where D is the dimensionality of the space. The homotopy classes of this mapping consist of configurations that can be continuously transformed into one another and form the $(D-1)$ th homotopy group $\pi_{D-1}(\mathcal{M})$ of \mathcal{M} . Furthermore, by restricting the mapping to subsets S^n of the S^{D-1} at infinity, where $n < D-1$, we obtain the lower homotopy groups $\pi_n(\mathcal{M})$.

Because the elements of the homotopy groups are invariant under continuous deformations, a field configuration that corresponds to a non-trivial element of any $\pi_n(\mathcal{M})$ with $n \leq D - 1$ cannot be continuously transformed into the vacuum solution. Within each homotopy class, there is a field configuration with minimal energy, and that configuration is necessarily a static solution of the field equations. However, it has typically a higher energy than the vacuum. In $D = 3$ dimensions, configurations with non-trivial 0th, 1st and 2nd homotopies correspond to domain walls, vortex lines (strings) and monopoles, respectively.

As an example, let us consider the $U(1)$ symmetric theory (4) and a field configuration of the form $\phi(r, \varphi, z) = |\phi(r)| \exp(i\varphi)$ in cylindrical coordinates where φ is the azimuth angle. A configuration like this cannot be continuously transformed into a vacuum solution, because the path of ϕ at the infinity corresponds to a non-trivial element of the first homotopy group $\pi_1(\mathcal{M})$. If we want ϕ to be continuous, it must vanish at $r = 0$, and this costs energy. Therefore we have a classical solution that corresponds to a line-like object, a vortex line.

The topology of the vacuum manifold follows directly from the symmetry breaking pattern. Because different vacua are characterized by different values of ϕ , \mathcal{M} is homeomorphic to the set $G(\phi)$ of all the possible values that can be obtained from ϕ by symmetry transformations. However, since the transformations in the unbroken subgroup H leave ϕ unchanged, \mathcal{M} is homeomorphic to the coset space G/H rather than the full group G . Thus, the homotopy groups $\pi_n(G/H)$ tell what types of topological defects exist in the theory.

In smooth configurations, which are not necessarily solutions of the classical field equations, we can identify the topological defects by calculating the element of $\pi_n(\mathcal{M})$ to which the behaviour of the field ϕ on a closed surface of dimensionality n corresponds. If this winding number is non-trivial, the surface must enclose a topological defect. In the above example with $G = U(1)$, the winding number along a closed curve C would be

$$N_W(C) = \frac{1}{2\pi} \oint_C d\vec{r} \cdot \vec{\nabla} \theta \equiv \frac{1}{2\pi} \Delta\theta, \quad (6)$$

where $\theta = \arg \phi$ is the phase angle of the order parameter field ϕ .

2.3. Defects in gauge theories

In gauge field theories, the discussion of the vacuum manifold becomes more subtle. A gauge transformation can be used to move the field anywhere in \mathcal{M} at each point in space-time independently of all other space-time points. For instance, it is always possible to carry out a gauge transformation into the *unitary gauge* in which the direction of the order parameter is the same everywhere. This does not by any means imply that there cannot be any topological defects in gauge theories, because the transformation also changes the gauge field. In fact, topological defects typically manifest themselves in the unitary gauge as non-physical gauge field singularities similar to the Dirac string in the Dirac monopole configuration.

6 Formation of topological defects in gauge field theories

A simple example of a defect in a gauge theory is the Nielsen-Olesen vortex¹⁷ in the Abelian Higgs model. This model is a gauge invariant generalization of the global U(1) theory in Eq. (4), and its Lagrangian is

$$\mathcal{L} = -\frac{1}{4}F_{\mu\nu}F^{\mu\nu} + D_\mu\phi^*D^\mu\phi - V(|\phi|). \quad (7)$$

The Nielsen-Olesen solution can be written in the form

$$\phi(r, \varphi, z) = ve^{iN_W\varphi}f(\lambda/e^2, evr), \quad A^i(r, \varphi, z) = -\frac{N_W}{er}\hat{\varphi}^i a(ev), \quad (8)$$

where v is the minimum of $V(|\phi|)$, N_W is an integer and $a(x)$ and $f(x)$ are functions, which must be determined numerically. They vanish at $x \rightarrow 0$ and approach unity exponentially at $x \rightarrow \infty$. If we calculate the total magnetic flux carried by the vortex, we find

$$\Phi = \lim_{R \rightarrow \infty} \oint_{|\vec{r}|=R} d\vec{r} \cdot \vec{A} = -\lim_{R \rightarrow \infty} 2\pi R \frac{N_W}{eR} a(evR) = -N_W \frac{2\pi}{e}, \quad (9)$$

which means that the magnetic flux is a multiple of the *flux quantum* $\Phi_0 = 2\pi/e$. The Abelian Higgs model is very similar to the Ginzburg-Landau theory of superconductivity,¹⁹ and in that context, the Nielsen-Olesen vortices are known as Abrikosov flux tubes.

An important property of the Nielsen-Olesen solution is that the energy density decreases exponentially at large r . In the global theory (4), the energy density around a vortex has a power-law decay $1/r^2$ because of the gradient term, but in the gauge theory it is mostly cancelled by the gauge field contribution to the covariant derivative $\vec{D}\phi$. Therefore, the energy per unit length of a vortex, *i.e.*, the tension, is finite in the gauge theory but logarithmically divergent in the global theory. This has the further implication that the interaction of two gauge vortices is exponentially suppressed at long distances, whereas global vortices have long-range interactions.

The interaction between two vortices is attractive if $\lambda/e^2 < 1/2$ and repulsive if $\lambda/e^2 > 1/2$.¹⁸ These cases correspond to type-I and type-II superconductors, respectively.¹⁹ Consequently, a solution with $|N_W| > 1$ is only stable if $\lambda/e^2 < 1/2$. In the special case $\lambda/e^2 = 1/2$, which is known as the Bogomolnyi point, one can find the exact form of the functions $f(x)$ and $a(x)$, and calculate the vortex tension exactly.²⁰

Another important defect solution is the 't Hooft-Polyakov solution in the Georgi-Glashow model.^{21,22} The theory consists of a Higgs field ϕ in the adjoint representation of the SU(2) gauge group. The Lagrangian can be written as

$$\mathcal{L} = -\frac{1}{2}\text{Tr}F_{\mu\nu}F^{\mu\nu} + \text{Tr}[D_\mu, \phi][D^\mu, \phi] - m^2\text{Tr}\phi^2 - \lambda\text{Tr}\phi^4, \quad (10)$$

where $D_\mu = \partial_\mu + igA_\mu$ and $F_{\mu\nu} = (ig)^{-1}[D_\mu, D_\nu]$. Classically, the SU(2) symmetry is broken into U(1) when m^2 is negative. The monopole solution has the form^{21,22}

$$\phi = \frac{\vec{\sigma} \cdot \vec{r}}{gr^2} H(gvr), \quad A^i = \frac{\vec{\sigma} \times \vec{r}}{gr^2} [1 - K(gvr)], \quad (11)$$

where $H(x)$ and $K(x)$ are functions which must be determined numerically and which behave asymptotically as $H(x) \sim x$ and $K(x) \rightarrow 0$. Going to the unitary gauge $\phi \propto \sigma^3$, we can see that the solution acts as a source for the magnetic field that corresponds to the residual $U(1)$ symmetry.²¹

Similar monopoles are also present if the group G that is broken is more complicated but has an $SU(2)$ subgroup that is broken into $U(1)$. In particular, practically any grand unified theory (GUT) predicts the existence of magnetic monopoles.²³ The masses of these monopoles would be around the GUT scale, which explains why they have not been observed in experiments. However, if the temperature of the universe was initially above the GUT scale, monopoles should have been formed in the phase transition in which the GUT symmetry group broke down into $SU(3) \times SU(2) \times U(1)$. This would have had disastrous effects for the later evolution of the universe. Therefore, it is commonly believed that if monopoles were formed, they were diluted away by a subsequent period of cosmological inflation.²⁴

3. Field theories at high temperatures

3.1. Equilibrium

In Section 2, we discussed only classical solutions and smooth field configurations, but in general, we shall be interested in phase transitions that start from a thermal equilibrium state. The density operator in thermal equilibrium at temperature $T = 1/\beta$ is $\rho \propto \exp(-\beta H)$, where H is the Hamiltonian. From this, we can in principle calculate the expectation value of any observable X ,

$$\langle X \rangle = \text{Tr} \rho X. \quad (12)$$

For practical calculations involving only static equilibrium quantities, it is often easier to use the imaginary time formalism, in which the observables are expressed as Euclidean path integrals²⁵

$$\langle X \rangle = Z^{-1} \int D\phi \exp \left(- \int_0^\beta d\tau \int d^3x \mathcal{L}_{\text{Eucl}}[\phi(\tau, \vec{x})] \right) X[\phi(0, \vec{x})] \quad (13)$$

and the partition function Z normalizes the result in such a way that $\langle 1 \rangle = 1$. The path integral has a similar form in gauge field theories as well, although the temporal component A_0 of the gauge field needs a special treatment.²⁶

In the high-temperature limit $\beta \rightarrow 0$, the compact imaginary time dimension shrinks to a point. Therefore, at high temperatures, the state of the system is well approximated by a three-dimensional path integral²⁷

$$\langle X \rangle = Z^{-1} \int D\phi \exp \left(-\beta \int d^3x \mathcal{L}_{3D}[\phi(\vec{x})] \right) X[\phi(\vec{x})]. \quad (14)$$

This approximation is called *dimensional reduction*, and it has been used very successfully in the study of the electroweak phase transition.^{28,29} The resulting path

integral has exactly the same form as the corresponding expectation value in classical statistical physics if we replace \mathcal{L}_{3D} by the classical Hamiltonian.

In thermal equilibrium, the state of the system is specified by the expectation values of all the observables. In a finite volume, these expectation values possess the same symmetries as the Lagrangian, and therefore all observables that transform covariantly under symmetry transformations vanish. However, in the thermodynamic limit, *i.e.*, in infinite volume, they may obtain non-zero expectation values, which signals that the symmetry is spontaneously broken. It depends on the parameters whether this happens, and the partition function of the system is non-analytic at the boundary between unbroken and broken symmetries. In other words, the system has a phase transition.

In the classical zero-temperature case discussed in Section 2, it was easy to determine whether a symmetry was broken by simply finding the global minimum of the potential. In the thermal case (or in the zero-temperature quantum case), we can define an effective potential,³⁰ which has the same property, by

$$V_{\text{eff}}(\varphi) = -\frac{T \ln \langle \delta(\bar{\phi} - \varphi) \rangle}{V}, \quad (15)$$

where $\bar{\phi} = V^{-1} \int d^3x \phi$. This corresponds to the free energy density of a micro-canonical system in which the volume average of the order parameter ϕ is fixed to the value φ . Because the free energy is minimized in thermal equilibrium, the minimum of the potential shows the equilibrium state of the system.

In perturbation theory, the effective potential can be calculated as a sum of one-particle irreducible (1PI) vacuum diagrams expanded around the desired value of ϕ .³⁰ In the global quantum theory (4), the one-loop effective potential is

$$\begin{aligned} V_{\text{eff}}(\varphi) &= V(\varphi) + \frac{T^2}{24} \left[\sum_i m_i^2(\varphi) + O(m(\varphi)^3/T) \right] \\ &= V(\varphi) + \frac{1}{6} \lambda T^2 |\varphi|^2 + \frac{m^2 T^2}{12} + O(m(\varphi)^3 T). \end{aligned} \quad (16)$$

This contribution increases the effective mass of ϕ from m^2 to $m^2 + \lambda T^2/3$. Therefore, even if the symmetry is broken at zero temperature, *i.e.*, $m^2 < 0$, it will be restored when the temperature becomes high enough $T > T_c \approx (-3m^2/\lambda)^{1/2}$.

In gauge field theories, it is straightforward to show that the gauge invariance is never spontaneously broken,³¹ but this does not mean that there cannot be phase transitions. In a fixed gauge, we can calculate $V_{\text{eff}}(\varphi)$ perturbatively. If the Higgs self-coupling λ is much less than the gauge coupling g^2 , this computation is believed to be reliable and produces a non-analytic cubic term $\propto |\varphi|^3$.^{32,33} This means that at a certain temperature T_c , there are two degenerate vacua corresponding to zero and non-zero values of φ . Consequently, the expectation value of ϕ jumps discontinuously from zero to a non-zero value when the temperature decreases, *i.e.*, there is a first-order phase transition.

When $\lambda \gg g^2$, perturbation theory becomes unreliable, and the line of first-order transitions ends in a second-order point. In some cases, the transition disappears completely at higher λ , and the phases are smoothly connected.³⁴ In others, a second-order transition survives. This happens, for instance, in the Abelian Higgs model; the transition at large λ/e^2 has its most natural description in terms of a dual theory, whose fundamental degrees of freedom are Nielsen-Olesen vortices.^{35,36}

3.2. Non-equilibrium

Formally, the time evolution of a quantum field theory is given by the operator equation of motion

$$i\frac{\partial X}{\partial t} = [X, H]. \quad (17)$$

If H is a constant in time, the system remains in thermal equilibrium, and if H depends on time, we obtain non-equilibrium evolution. The problem is that X is an operator, and therefore it is extremely difficult to solve Eq. (17) in any non-trivial field theory, and we have to resort to approximations, which are discussed in more detail in Section 6.

4. First-order phase transitions

If the transition is of first order, the symmetric phase remains metastable even slightly below the critical temperature. The effective potential has two minima, and at the transition point, the one corresponding to the broken phase becomes the global minimum. After that, there is a finite probability per unit volume that the thermal fluctuations throw the system over the potential barrier from the metastable symmetric phase into the true, broken minimum. It is more probable that this happens in only a small region of space. The boundaries around this bubble of broken phase cost energy, but the potential energy inside it is lower than in the symmetric phase. If the bubble is large enough, the contribution from the potential energy becomes larger than that from the bubble wall, and the bubble starts to grow.

We can estimate the nucleation rate of these bubbles by calculating the energy E_c of a critical bubble, *i.e.*, the lowest-energy bubble that starts to grow instead of shrinking away.^{37,38,39} This gives the exponential suppression of the nucleation rate, $\Gamma_{\text{nucl}} \propto \exp(-\beta E_c)$, and therefore a reasonable order-of-magnitude estimate as long as $\beta E_c \gg 1$. Calculating the prefactor requires significantly more work.⁴⁰

In a large system, many bubbles are nucleated at different points in space, and when the bubbles grow, they eventually coalesce and fill the whole space, thus completing the transition. The bubble walls are typically moving relatively slowly⁴¹ and are preceded by shock waves, which heat up the system.⁴² This suppresses the further nucleation of bubbles nearby.

4.1. Global theories

When a symmetry breaks, no point on the vacuum manifold \mathcal{M} is preferred over any other. In a first-order transition, it is therefore a very reasonable assumption that the direction of symmetry breaking is uncorrelated between different bubbles. Inside a single bubble, on the other hand, it is energetically preferable for the order parameter field ϕ to be constant. If the vacuum manifold \mathcal{M} is not connected, *i.e.*, $\pi_0(\mathcal{M}) \neq 1$, ϕ may belong to different connected parts inside two neighbouring bubbles, and when the bubbles meet, a domain wall is formed between them.⁴³

If \mathcal{M} is connected but not simply connected, *i.e.*, $\pi_1(\mathcal{M}) \neq 1$, then ϕ can always relax to a constant after a collision of two bubbles. However, if a third bubble hits the first two before this has happened, a vortex can be formed. Imagine, for instance, that $G=U(1)$ and inside the three bubbles the phase angle θ of the order parameter ϕ has the values θ_1 , θ_2 and θ_3 . It is common to assume the *geodesic rule*,^{1,44} *i.e.*, that when the phase angle interpolates between the values inside two bubbles, it always uses the shortest path in the vacuum manifold. It may then happen that the path that connects θ_1 to θ_2 to θ_3 and finally to θ_1 winds around the vacuum manifold, in which case the order parameter cannot relax to a constant everywhere and a vortex is formed. Similarly, we can see that in theories with $\pi_2(\mathcal{M}) \neq 0$, collisions of four bubbles may lead to formation of monopoles.

In this simple picture, the probability of forming a topological defect in a bubble collision depends essentially only on the geometry of the collision and on the geometry of the symmetry group. Therefore, we can conclude that the typical distance between the vortices is proportional to the typical separation between the bubble nucleation sites d_{nuc} . We can characterize the density of topological defects whose codimensionality is D_{co} by the number density n of points where a defect crosses a subspace of dimensionality D_{co} . According to the above discussion, it behaves as

$$n \approx d_{\text{nuc}}^{-D_{\text{co}}}. \quad (18)$$

In practice, D_{co} is 1 for domain walls, 2 for vortices and 3 for monopoles. For instance, the number density of vortices per unit cross-sectional area is predicted to be $n \approx d_{\text{nuc}}^{-2}$.

The probabilities of forming defects in symmetric collisions of bubbles have been calculated by Prokopec.⁴⁵ Although bubble nucleation is essentially a random event and therefore the bubble nucleation events are more or less evenly distributed in space and time, it was customary in early studies to assume that all bubbles were nucleated simultaneously in a regular lattice.⁴⁴ Obviously, the form of the lattice then affects the results.⁴⁶ One attempt to avoid this problem was the “lattice-free” approach^{47,48} in which the bubble locations are random.

For a more accurate treatment, the field dynamics must be taken into account. If the bubbles do not collide simultaneously, the probability of forming a defect decreases, because the order parameter may already have equilibrated before the third bubble hits the first two.⁴⁹ Furthermore, the growth of the bubbles is typically much slower than the speed of light because of the friction caused by the hot plasma that fills the space at high temperatures.⁴¹ This allows more time for the phase

equilibration between the first two bubbles to happen and therefore decreases the probability of forming a defect even further,⁵⁰ although it also means that a larger fraction of space is in the symmetric phase at any given time and therefore the total number of bubble nucleation events is larger.

4.2. Gauge field theories

In gauge field theories, the above picture cannot be used directly, because the direction of the order parameter is not gauge invariant. In particular, we can always choose a gauge in which ϕ is equal in the two colliding bubbles. That led Rudaz and Srivastava⁵¹ to question the applicability of the geodesic rule in gauge theories.

The first detailed studies of the field dynamics in the Abelian Higgs model^{52,53} showed that this is not the case if the phase transition starts from a classical vacuum state. In order to treat the phase angles in a gauge-invariant way, Kibble and Vilenkin⁵³ introduced a gauge-invariant phase difference

$$\Delta_{\text{gi}}\theta = \int d\vec{r} \cdot \vec{D}\theta, \quad (19)$$

where $\vec{D}\theta = \vec{\nabla}\theta + e\vec{A}$. This cannot be used as a direct substitute for the phase angle difference defined in Eq. (6), because it depends on the path along which the difference is calculated and the phase difference around a closed curve is not quantized. Furthermore, $\Delta_{\text{gi}}\theta$ around a classical vortex configuration is zero, not 2π as in the global case, and therefore the gauge-invariant phase difference by itself cannot be used to locate vortices.

Let us first consider a collision of two bubbles in a classical vacuum, where the magnetic field vanishes, *i.e.*, $\vec{B} = \vec{\nabla} \times \vec{A} = 0$. In this case, we can choose the gauge $\vec{A} = 0$, which means that the gauge invariant phase difference is simply the ordinary phase difference. If we denote it by θ_0 , a circular magnetic flux ring with flux $\Phi = \int d\vec{S} \cdot \vec{B} = \theta_0/e$ is formed around the point of their collision, because the phase difference induces an electric current from one bubble to another^{51,53} (see Fig. 1a). In a simultaneous collision of three bubbles, all of the three collisions are at first totally independent and in each of them a flux ring like this is formed. Before the collision is complete, a hole remains at the middle of the collision, and the total flux Φ_{tot} through this hole is the sum of the gauge invariant phase differences divided by e , *i.e.*, $\Phi_{\text{tot}} = \Delta_{\text{gi}}\theta/e$. When the hole shrinks, this flux is squeezed into a Nielsen-Olesen vortex of winding $N_W = e\Phi_{\text{tot}}/2\pi = \Delta_{\text{gi}}\theta/2\pi$. Because in the $\vec{A} = 0$ gauge, $\Delta\theta = \Delta_{\text{gi}}\theta$, this is equal to the result (6) predicted by a naive application of the geodesic rule.

However, in practice the transition starts from a thermal state, and Kibble and Vilenkin⁵³ pointed out that then the fluctuations of the magnetic field are always present. These fluctuations change the above picture, leading to a violation of the geodesic rule. More precisely, if the area between the bubbles is A , the typical magnetic flux will be $\Phi_T \sim \sqrt{AT}$. Suppose for simplicity that the flux is peaked around the centre of the collision so that it does not affect the individual two-bubble

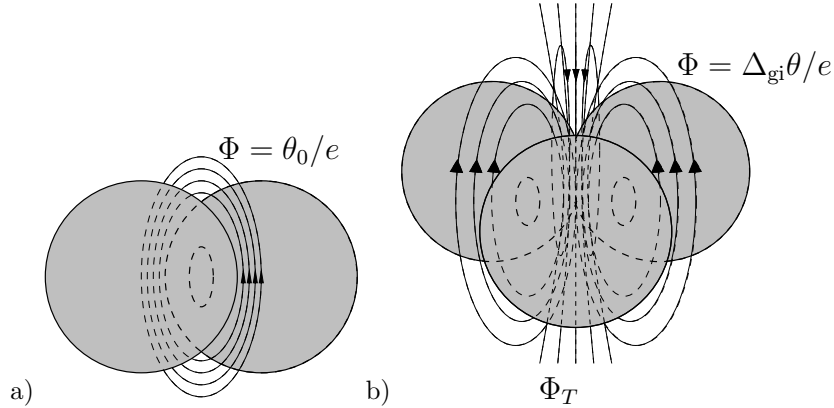


Figure 1: Bubble collisions in the Abelian Higgs model. a) In the classical vacuum $\vec{A} = 0$, a collision of two bubbles with a phase difference θ_0 forms a ring of magnetic field. b) In a collision of three bubbles, the flux rings and the initial flux Φ_T between the bubbles contribute to the total flux which turns into vortices.

collisions. Then, the three flux rings are again formed, and they merge with the initial flux Φ_T , which is trapped between the bubbles (see Fig. 1b). This leads to the formation of a vortex with winding

$$N_W = (\Delta_{gi}\theta - e\Phi_T)/2\pi = N_W^0 - e\Phi_T/2\pi, \quad (20)$$

where N_W^0 is the winding number predicted by $\Delta_{gi}\theta$ alone. Note that N_W^0 is typically not an integer, but N_W always is. If the bubbles are far apart, Φ_T can be very large, and therefore vortices with very high windings can form.

The generalization of the above picture to non-Abelian gauge field theories is still an open question. It is not at all obvious what the analogue of the magnetic flux Φ_T in the case of, say, 't Hooft-Polyakov monopoles is. Furthermore, because of confinement, a non-Abelian gauge field theory cannot be approximated by a free field theory. In this paper, we shall therefore only consider Abelian gauge field theories.

5. Continuous phase transitions

The dynamics of first-order phase transitions are simplified by the hierarchy between the bubble nucleation rate and other time scales. Furthermore, because of the metastability we were allowed to assume that the temperature is initially below T_c and that it remains constant during the phase transition. In continuous transitions, the dynamics of the transition depends on how, and especially how rapidly, the phase transition line is crossed.

A continuous phase transition is usually of second order, which means that the second derivative of the free energy is discontinuous and at least one correlation length diverges. Most commonly, these transitions are associated with a spon-

taneous breakdown of a symmetry, but opposite examples are also known. For instance, in the two-dimensional XY model,⁵⁴ the classical analysis *à la* Section 2.1 would suggest that the symmetry gets broken, but a proper treatment shows that this is not the case, because a continuous symmetry cannot be broken in a two-dimensional theory.^{55,56} A similar theorem applies to gauge field theories in any number of dimensions,³¹ and therefore depending on the model, the phase transitions can range from first-order transitions³² to smooth crossovers.³⁴

In the setup we shall consider, the system is initially in thermal equilibrium in the symmetric phase. The system is forced to undergo a phase transition by changing one of the parameters continuously through the phase transition line at a rate characterized by the *quench timescale* τ_Q . In different cases, the parameter that is changed can be, for instance, a coupling constant, the mass parameter, the scale factor of the universe or the pressure. Although the precise way the parameters are changed certainly affects the detailed dynamics, the qualitative picture and the order-of-magnitude estimates are believed to be unaffected.

The defects are counted after the transition when they have become well-defined objects. If the interaction between the defects has a short range, this can be done very reliably by letting the system equilibrate locally to the low temperature so that thermal fluctuations are negligible and counting the defects only after that. When the interaction has a long range, the number of defects after the transition has a certain ambiguity depending on how they are counted, but because we are only interested in orders of magnitude, we shall ignore these problems.

In most theoretical studies, it is assumed that the phase transition is homogeneous, but in a real experiment any method of cooling or changing some external parameters in some other way always leads to inhomogeneities, which may be important for defect formation.^{57,58} We shall not discuss these complications here.

5.1. Global theories

The overall picture of defect formation in second-order transitions in global theories is in many ways similar to the first-order transitions discussed in Section 4. After the transition, the order parameter can only be correlated at distances less than some finite correlation length $\hat{\xi}$ and therefore we can replace the bubbles in the analysis with correlated domains of radius $\hat{\xi}$.^{43,1} When we replace d_{nucl} by $\hat{\xi}$ in Eq. (18), we find

$$n \approx \hat{\xi}^{-D_{\text{co}}}. \quad (21)$$

In cosmology, we can state the ultimate upper limit for $\hat{\xi}$ as the age of the universe,⁴³ but in practice $\hat{\xi}$ is always much shorter than that.

The early suggestion¹ was to identify $\hat{\xi}$ with the correlation length at the Ginzburg temperature T_G defined by

$$\frac{\Delta V(T_G)}{T_G} \xi(T_G)^3 = 1. \quad (22)$$

Below T_G , the thermal fluctuations become incapable of restoring the symmetry in

patches larger than the correlation length. This would mean that the final number density of defects is independent of the quench timescale τ_Q . However, symmetry restoration in a patch of radius $\hat{\xi}$ can only form vortex loops of radius less than $\hat{\xi}$ or monopole-antimonopole pairs with separation less than $\hat{\xi}$, and these are unstable configurations which quickly annihilate when the symmetry gets broken again. The defects that survive after the transition must have therefore been formed at an earlier stage. Nevertheless, the Ginzburg temperature still has the significance that individual defects can only be identified reliably at $T < T_G$.

The attempt to use the Ginzburg temperature to estimate the defect density also ignores the fact that reordering the order parameter at long distances takes time.⁵⁹ Therefore, even if it were energetically possible, it may not have time to happen in a rapid transition. Instead, the relevant length scale is actually determined as a compromise between the tendency of ordering the fields at long distances and the finite time available for that process. This argument was used by Zurek to derive a more realistic estimate for the defect density.^{5,60}

A characteristic property of second-order phase transitions is that the correlation length of the order parameter diverges at the transition point with some critical exponent ν , *i.e.*, $\xi(T) \approx \xi_0 |\epsilon|^{-\nu}$, where $\epsilon(T) = (T_c - T)/T_c$ and the exponent ν depends only on the universality class of the model. However, in practice, ξ cannot grow arbitrarily fast, because at least it is constrained by causality to change slower than the speed of light.⁵⁹ If the transition takes place at a finite rate, say, $\epsilon = t/\tau_Q$, then eventually a point is reached at which the true correlation length cannot keep up with the equilibrium correlation length $\xi(T)$ at the same temperature. After that, the dynamics of the system cease to be adiabatic.

In reality, other effects make the maximum growth rate of the correlation length much less than the speed of light. Zurek⁵ assumed that the relevant dynamics of the system can be characterized by a relaxation timescale $\tau(T)$, which also diverges at the transition point in equilibrium, but typically with a different critical exponent, $\tau \approx \tau_0 |\epsilon|^{-\mu}$.

Zurek's estimate is based on the idea that when the transition is approached from the symmetric phase, the dynamics of the system eventually become too slow to stay adiabatic and the maximum correlation length $\hat{\xi}$ is roughly the correlation length at that time. More precisely, he used the condition $\tau(\hat{t}) = |\hat{t}|$ to signal the breakdown of adiabaticity, which implies

$$\hat{t} \approx -(\tau_0 \tau_Q^\mu)^{1/(1+\mu)}. \quad (23)$$

The maximum correlation length is then

$$\hat{\xi} \approx \xi_0 \left(\frac{\tau_Q}{\tau_0} \right)^{\nu/(1+\mu)}. \quad (24)$$

The critical exponents μ and ν depend on the system, and at intermediate length scales, they may be different from their true, asymptotic values. Laguna and

Zurek⁶¹ have discussed two special cases, the overdamped case with $\mu = 1$ and the underdamped case with $\mu = 2$. In mean-field theory $\nu = 1/2$, implying

$$\hat{\xi}_{\text{MF}}(\tau_Q) \approx \begin{cases} \xi_0 (\tau_Q/\tau_0)^{1/4}, & (\text{overdamped}) \\ \xi_0 (\tau_Q/\tau_0)^{1/3}. & (\text{underdamped}) \end{cases} \quad (25)$$

In any case, causality constrains $\mu \geq \nu$.

Finally, let us clarify the meaning of the correlation length by discussing it from another viewpoint. If we denote the dimensionality of the order parameter by N , there are N orthogonal elementary excitations. In the symmetric phase, they are all degenerate, *i.e.*, have the same correlation length. Therefore it makes sense to talk about “the correlation length” ξ . However, in equilibrium in the broken phase, only one of these correlation lengths is finite, namely the one that corresponds to the modulus of the order parameter. The direction of the order parameter becomes a Goldstone mode with an infinite correlation length.

After a rapid phase transition, both correlation lengths are initially roughly equal, ξ_{mod} , which corresponds to the modulus of the order parameter, and ξ_{GS} , which corresponds to the Goldstone modes. However, ξ_{mod} starts to decrease rapidly, and because it determines the size of the defect core, the defects become well-defined objects. On the other hand, ξ_{GS} characterizes the separation between the defects, since it is easy to see that defects cause disorder to the order parameter field at distances larger than their separation, but at shorter distances the direction of the order parameter is correlated. When the defect configuration evolves, defects annihilate, and ξ_{GS} approaches its infinite equilibrium value, albeit very slowly. This is another way of seeing why the maximum correlation length should determine the density of defects.

In the following we shall call the above scenario the *Kibble-Zurek mechanism*. It is believed to be generally valid in phase transitions in which a global symmetry is broken. During the recent years, it has been tested extensively in numerical simulations and condensed matter experiments, which we shall discuss in more detail in Sections 6 and 7, respectively.

5.2. Gauge field theories

As in the case of first-order phase transitions, the gauge fields were long thought to be irrelevant for defect formation.¹⁵ This view was even supported by early numerical simulations,⁶² which showed a good agreement with the Kibble-Zurek mechanism. It is now understood that this was because the initial temperature was very low in them.^{14,63}

Just like in the case of first-order transitions, thermal fluctuations of the magnetic field are present at any non-zero initial temperature, and they have an important effect on the dynamics. As discussed in Section 4.2, the magnetic flux that originates in thermal fluctuations can get trapped between the bubbles in three-bubble collisions in a first-order phase transition, leading to the formation of vortices with higher windings.⁵³ In a similar way, Zurek⁶⁴ argued that when a

superconductor loop is rapidly quenched into the superconducting phase, magnetic flux can get trapped inside even when the transition is continuous. In that case, it cannot be interpreted as a vortex, though, because its core is outside the system.

The dynamics are more complicated in the “bulk” case, in which the system fills the whole space. It was shown by Hindmarsh and Rajantie¹⁴ that even in a continuous phase transition, the long-wavelength thermal fluctuations of the magnetic field freeze out in the phase transition and form vortices. More recently, similar conclusions were also reached by Stephens *et al.*,⁶³ who studied instantaneous quenches. We shall call this way of forming vortices the *flux trapping* mechanism.

The starting point of the flux trapping mechanism is that in the Coulomb (normal) phase, there are fluctuations of the magnetic field with arbitrarily long wavelengths. The simplest approximation is to treat the Coulomb phase as a vacuum, in which case these thermal fluctuations are simply blackbody radiation. Provided that the coupling to the other fields is weak, the fluctuations are Gaussian and uncorrelated, and the width of the Gaussian distribution is proportional to the temperature and independent of the momentum.

The local magnetic field \vec{B} is given by $\vec{\nabla} \times \vec{A}$. If we define its two-point correlation function $G(k)$ as

$$\langle B_i(\vec{k}) B_j(\vec{k}') \rangle = \left(\delta_{ij} - \frac{k_i k_j}{k^2} \right) (2\pi)^3 \delta(\vec{k} + \vec{k}') G(k), \quad (26)$$

we have in the free-field approximation

$$G(k) = T. \quad (27)$$

Of course, neither the high-temperature phase of the Abelian Higgs model nor the normal phase of a superconductor is exactly a vacuum, and therefore Eq. (27) obtains corrections, which suppress the fluctuations. Near the transition point, critical fluctuations also change the correlator, and the magnetic field obtains a non-trivial anomalous dimension. Therefore we can generally assume that in the limit $k \rightarrow 0$,

$$G(k) \propto k^\eta, \quad (28)$$

with some anomalous dimension $0 \leq \eta < 2$.

In the Higgs (superconducting) phase, long-range fluctuations are suppressed, and the equilibrium two-point function becomes

$$G(k) \approx \frac{T k^2}{k^2 + m_\gamma^2}, \quad (29)$$

where m_γ is the inverse correlation length of the magnetic field,

$$m_\gamma \approx ev \approx \sqrt{\frac{e^2}{\lambda} (-m^2)}. \quad (30)$$

When the system goes through the phase transition, each Fourier mode of the magnetic field must change its amplitude from Eq. (27) into Eq. (29) in order to

remain in equilibrium. However, it has only a finite amount of time available for this, and if it reacts too slowly, it falls out of equilibrium. The crucial point is that the modes with long wavelengths react slower and this is therefore more likely to happen to them. We denote by $\tau(k)$ the time scale within which a Fourier mode with wavenumber k can change, and in the vacuum approximation it is simply the inverse frequency, $\tau(k) \approx k^{-1}$. More realistically, the time scale may be determined by the conductivity of the material, or by plasma effects, but in any case, $\tau(k) \rightarrow \infty$ as $k \rightarrow 0$, which means that there is always some critical wavelength $\hat{\xi}$ so that modes with longer wavelengths (*i.e.*, $k \lesssim \hat{\xi}^{-1}$) cannot adjust but fall out of equilibrium.

What this means is that after the phase transition, the distribution of the magnetic field at distances longer than $\hat{\xi}$ is the same as it was before the transition. In particular, we can calculate the typical (rms) magnetic flux through a loop of radius $\hat{\xi}$ using Eq. (28). The result depends on the dimensionality D of the space, and assuming $\eta = 0$, we find¹⁴

$$\Phi_{\hat{\xi}} \approx T^{1/2} \hat{\xi}^{2-D/2}. \quad (31)$$

As the modes with wavelength less than $\hat{\xi}$ were able to equilibrate, the field configuration inside this loop has relaxed into its minimum energy configuration, which is a cluster of

$$N_{\hat{\xi}} \approx \Phi_{\hat{\xi}} / \Phi_0 \approx \frac{e}{2\pi} T^{1/2} \hat{\xi}^{2-D/2} \quad (32)$$

vortices, each having the same sign. Dividing this by the area of the loop, we find the number density of vortices formed in the transition,

$$n \approx \frac{N_{\hat{\xi}}}{\hat{\xi}^2} \approx \frac{e}{2\pi} T^{1/2} \hat{\xi}^{-D/2}. \quad (33)$$

It is important to note that the dependence on $\hat{\xi}$ is different from the prediction (18) of the Kibble mechanism, and that the density increases with increasing temperature and increasing gauge coupling constant. In particular, Eq. (33) vanishes in the global limit $e \rightarrow 0$, and only the Kibble-Zurek mechanism remains.

It has been argued by Stephens *et al.*⁶³ that if the phase transition is very rapid, the picture becomes more complicated. In the Higgs phase, the magnetic field can only penetrate the system if it exceeds the critical field B_{c1} . Near the transition, B_{c1} vanishes, but if the quench is instantaneous, we can assume that it jumps discontinuously to a non-zero value. This would mean that no vortices are formed in regions where the flux density is lower than B_{c1} .

In order to use Eq. (33) to predict the number density of defects, we must be able to calculate $\hat{\xi}$. Hindmarsh and Rajantie¹⁴ argued that this can be found by using an adiabaticity condition, which balances the rate at which the equilibrium two-point function $G(k)$ of a given Fourier mode must change in order to remain in equilibrium with the dynamical time scale of the same mode,

$$\left| \frac{d \ln G(\hat{k})}{dt} \right| = \tau^{-1}(\hat{k}). \quad (34)$$

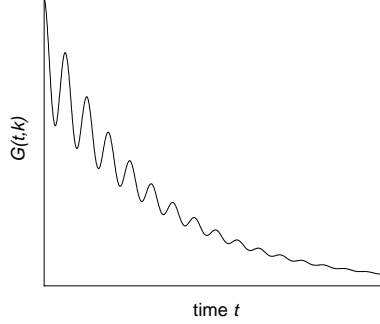


Figure 2: Typical form of the real-time correlator $G(t, k) \propto \langle \vec{B}(0, \vec{k}) \vec{B}(t, -\vec{k}) \rangle$ of the magnetic field. It is a linear combination of an exponentially decreasing Landau damping contribution $\exp(-\gamma_L t)$ and an oscillatory plasmon contribution $\exp(-\gamma_p t) \cos(\omega_p t)$. At long wavelengths, $\gamma_L \ll \omega_p, \gamma_p$,⁶⁵ and therefore γ_L determines the time $\tau \sim \gamma_L^{-1}$ when $G(t, k)$ vanishes. This is the time needed for a perturbation of the magnetic field to equilibrate.

Furthermore, they argued that in the relativistic case, $\tau(k)$ is determined by the Landau damping rate⁶⁵ γ_L [see Fig. 2]

$$\tau^{-1}(k) = \gamma_L(k) \approx \frac{4k^3}{\pi m_D^2}. \quad (35)$$

Assuming that $G(k)$ is given by Eq. (29), where $m^2 = -\delta m^2 t / \tau_Q$, we find that Eq. (34) becomes

$$\frac{e^2}{\lambda} \frac{\delta m^2}{\tau_Q} \frac{1}{\hat{k}^2} \approx \frac{4\hat{k}^3}{\pi m_D^2}, \quad (36)$$

from which we obtain

$$\hat{\xi} \propto \hat{k}^{-1} \propto \tau_Q^{1/5}. \quad (37)$$

Using Eq. (33), we can then see that the number density of vortices per unit cross-sectional area behaves in three spatial dimensions as

$$n \propto \tau_Q^{-0.3}. \quad (38)$$

However, this result is not valid at very large τ_Q .⁶⁵ When $k \ll e^2 T$, non-perturbative effects change the form of the equilibrium correlator $G(k)$, leading to a non-trivial anomalous dimension η . Furthermore, at low k , it is conductivity σ rather than Landau damping that determines the rate of exponential damping γ_L and this changes its behaviour to $\gamma_L \approx k^2 / \sigma$.

It is obvious, too, that while the equilibrium equal-time correlator $G(k)$ is believed to be universal, the dynamics and therefore the relaxation time scale $\tau(k)$ are sensitive to the details of the system. This means that the power law may be different for, say, superconductors, although the mechanism itself is believed to be

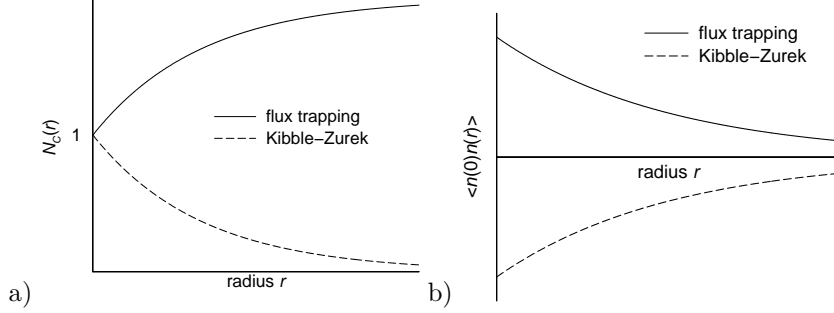


Figure 3: a) The behaviour of $N_C(r)$ defined in Eq. (39) as predicted by the flux trapping and Kibble-Zurek mechanisms. b) The form of the vortex-vortex correlation function $\langle n(0)n(r) \rangle$ as predicted by the flux trapping and Kibble-Zurek mechanisms.

valid. Finally, when applying Eq. (33) to a transition in a superconducting film, we have to be careful, because although the film itself is two-dimensional, the magnetic field extends to the third dimension as well.⁶⁶

5.3. Spatial distribution of topological defects

Because neither the Kibble-Zurek nor the flux trapping mechanism can give clear-cut predictions for the number density of topological defects formed in a phase transition unless we make certain, fairly strong assumptions about the dynamics, the number density itself is not a very good quantity for testing the mechanisms. Instead, we should look for signals that are truly qualitatively different in the two mechanisms, such as the spatial distribution of vortices after the phase transition. This has been emphasized by Digal *et al.*⁶⁷ who pointed out that the Kibble mechanism leads to strong negative vortex-vortex correlations.

A simple way of seeing that the two mechanisms predict very different spatial distributions is to look at the quantity $N_C(r)$,¹⁴ defined as the average winding number around a circle of radius r centred at the positive vortex. Formally, we may write it as the expectation value

$$N_C(r) = \left\langle n(\vec{x}) \frac{1}{2\pi} \oint_{|\vec{x}' - \vec{x}|=r} d\vec{x}' \cdot \vec{\nabla} \theta(\vec{x}') \right\rangle = \left\langle n(\vec{x}) \int_{|\vec{x}' - \vec{x}| \leq r} d^2 x' n(\vec{x}') \right\rangle, \quad (39)$$

where $n(\vec{x})$ is the winding number density at point \vec{x} . From the latter form we obtain

$$\frac{dN_C(r)}{dr} = 2\pi r \langle n(0)n(r) \rangle. \quad (40)$$

Let us first consider the Kibble-Zurek mechanism. The typical separation of vortices is given by $\hat{\xi}$, whereby we do not encounter any vortices of either sign at short distances, $r \ll \hat{\xi}$, as we increase r . However, when $r \gg \hat{\xi}$, this changes,

because we can write Eq. (39) in the form

$$N_C(r) = \frac{1}{2\pi} \oint_{|\vec{x}' - \vec{x}|=r} d\vec{x}' \cdot \left\langle n(\vec{x}) \vec{\nabla} \theta(\vec{x}') \right\rangle, \quad (41)$$

and by the definition of $\hat{\xi}$, the fields are uncorrelated at distance r . Therefore $\langle n(\vec{x}) \vec{\nabla} \theta(\vec{x}') \rangle = 0$, and consequently, $N_C(r) = 0$. Thus $N_C(r)$ must be a decreasing function of r , as shown in Fig. 3 by dashed lines. Using Eq. (40) this implies that there is a negative correlation between the vortices: Wherever there is a vortex, there is likely to be an antivortex nearby.

The distribution produced by the flux trapping mechanism is very different. As Eq. (32) shows, the vortices tend to form clusters of radius $\hat{\xi}$, each containing $N_{\hat{\xi}}$ vortices. Therefore, at short distances, $r \ll \hat{\xi}$, each new vortex encountered when r is increased typically has the same sign, and consequently $dN_C/dr > 0$. At long distances, $r \gg \hat{\xi}$, the vortex distribution is the same as the initial magnetic field distribution,

$$\langle n(0)n(r) \rangle \propto \langle B(0)B(r) \rangle_{\text{equilibrium}}. \quad (42)$$

In the vacuum approximation (27), the magnetic field is uncorrelated between different points. Therefore $\langle n(0)n(r) \rangle = 0$, and Eq. (40) shows that $dN_C/dr = 0$. This means that at distances less than $\hat{\xi}$, $N_C(r)$ is increasing, and near $\hat{\xi}$ it reaches a constant value. This is shown in Fig. 3 by solid lines. Using Eq. (40), we can also say that the vortices have positive correlations at short distances: Wherever there is a vortex, there is likely to be another one with the same sign nearby.

Thus, we have seen that there is a clear, qualitative difference in the vortex distributions formed by the two mechanisms. In practice, both mechanisms are believed to operate, but by measuring the form of the distribution, we can find out which one of them is dominant. This has already been done in numerical simulations, which are discussed in more detail in Section 6, but it can also be done fairly straightforwardly in superconductor experiments. This possibility is discussed in Section 7.4.

6. Theoretical methods for studying phase transition dynamics

Ideally, the Kibble-Zurek and flux trapping mechanisms could be easily tested numerically by solving the dynamics of the phase transition in some simple, yet non-trivial enough quantum field theory. However, exact analytical solutions for quantum dynamics are possible only in very simple special cases. Therefore, some approximations are unavoidable, and many different approaches have been attempted.

The methods are typically variants of either the Gaussian or the classical approximation. Examples of the first group are the linear approximation, in which interactions are neglected altogether and which corresponds to tree-level perturbation theory, and the Hartree approximation, which is essentially a tadpole resummation of the perturbative expansion. The advantage of these approaches is that we can, at least in a certain sense, keep the full quantum mechanical nature of the system.

The price we have to pay is that the self-interaction of the field is not described correctly, and therefore the approximations can only be valid at early times. For the same reason, the Gaussian approximations do not describe the thermal equilibrium state correctly near the transition and can therefore at best reproduce Eq. (24) with the mean-field exponents rather than with the true ones. Another weakness of the approach is that it is difficult to apply to more complicated theories, such as gauge field theories.

Classical approximation relies on the observation that in thermal equilibrium, long-wavelength modes have high occupation numbers and can therefore be assumed to behave classically. The most common realization of this idea is the time-dependent Ginzburg-Landau (TDGL) approximation, which consists of adding phenomenological noise and damping terms to the equations of motion. The main advantage of the classical approximation is that it describes the non-perturbative interactions of the long-wavelength modes correctly and, therefore, it also gives a correct description of the equilibrium state. However, it does not include any quantum effects and it is, after all, a purely phenomenological theory, which does not necessarily describe correctly the dynamics of the intended fundamental theory. We should also be careful with the renormalization of the model, because the classical field theory has different ultraviolet behaviour from the original quantum theory.

The hard-thermal-loop (HTL) approximation incorporates one-loop quantum corrections to the classical theory in order to avoid the weaknesses of the TDGL approach. It requires more resources than the classical approximation but is believed to approximate both the non-perturbative and the quantum mechanical aspects of the system correctly at reasonably long distances and time scales.

6.1. Linear approximation

The simplest approximation for the non-equilibrium dynamics is to approximate the system by a free field theory,⁶⁸ *i.e.*, to neglect all interactions. One advantage of this approach is that one can study the time evolution of the full density matrix and therefore address issues such as decoherence and classicality.⁶⁹

Let us consider a global $O(N)$ scalar field theory with the Lagrangian

$$\mathcal{L} = \frac{1}{2} \partial_\mu \phi_i \partial^\mu \phi_i - \frac{m^2}{2} \phi_i \phi_i - \frac{\lambda}{4} \phi_i \phi_i \phi_j \phi_j, \quad (43)$$

where $i, j \in \{1, \dots, N\}$. In the linear approximation, the equation of motion for each Fourier mode $\phi_i(k)$ becomes

$$\partial_0^2 \phi_i(k) = -(k^2 + m^2) \phi_i(k). \quad (44)$$

If $m^2 < 0$, the modes with $k < \sqrt{-m^2}$ are unstable and grow exponentially. This approximation works in an instantaneous quench with Gaussian initial conditions until

$$\langle \phi_i \phi_i \rangle = \int \frac{dk}{2\pi} |\phi_i(k)|^2 \approx -m^2/\lambda. \quad (45)$$

Because the interaction term is neglected altogether, the linear approximation does not describe topological defects at all, but it still shows how the long-wavelength modes grow during the early stages of the time evolution. Therefore, if we assume that the defect distribution is related to the field spectrum in some particular way, it can give some information about the topological defects formed in the transition. A popular assumption is to identify the zeroes of the field with topological defects. In the special case of a Gaussian field, every observable is given by the two-point function $G(x)$, and therefore the density of zeroes can also be written as^{70,71}

$$\langle n_0 \rangle = C \sqrt{\left| \frac{G''(x=0)}{G(x=0)} \right|}, \quad (46)$$

where the constant C depends on the dimensionality of the space and on the symmetry group.

In principle, the linear approximation can also be used for a time-dependent m^2 , but in practice the quench must be instantaneous,⁶⁸ because otherwise $\langle \phi_i \phi_i \rangle$ reaches $-m^2(t)/\lambda$ immediately and the approximation breaks down. Nevertheless, the approach has been generalized to a slowly varying m^2 by Karra and Rivers.^{72,73} In the case of a dissipationless (underdamped) field,⁷³ they found $\hat{\xi} \propto \tau_Q^{1/3}$, and in the overdamped case⁷⁴ $\hat{\xi} \propto \tau_Q^{1/4}$. Both of these results agree with Zurek's mean-field prediction (25).

Non-instantaneous quenches have also been studied in a stochastic (1+1)-dimensional theory in the linear approximation by Lythe⁷⁵ and Moro and Lythe.⁷⁶ In the overdamped case,⁷⁵ the density of kinks was $n \propto \tau_Q^{-1/4}$, which agrees with Zurek's mean-field prediction (25). In the underdamped case,⁷⁶ they found a logarithmic correction to Zurek's result, $n \propto \tau_Q^{-1/3} \ln \tau_Q$, and they were also able to calculate analytically the prefactors of the power law. On the other hand, Dziarmaga⁷⁷ has argued that the τ_Q dependence of the underdamped case should actually be $n \propto \tau_Q^{-1/2}$ in very slow quenches.

6.2. 2PI formalism

One widely used way of going beyond the linear approximation is to use the two-particle irreducible (2PI) effective action.^{78,79} It is a straightforward generalization of the ordinary effective action to the case of a field correlator. Let us, for instance, consider the two-point function $G(x, y) = \langle \phi^\dagger(x) \phi(y) \rangle$, assuming for simplicity that the expectation value $\langle \phi \rangle$ vanishes. We introduce an external source $K(x, y)$,

$$Z[K] = \text{Tr} \left[\rho \exp \left(\frac{i}{\hbar} \int dx dy K(x, y) \phi^\dagger(x) \phi(y) \right) \right]. \quad (47)$$

Then the two-point function is simply given by

$$G(x, y) = -i\hbar \frac{\partial \ln Z[K]}{\partial K(x, y)}. \quad (48)$$

The 2PI effective action $\Gamma[G]$ is defined as a Legendre transform

$$\Gamma[G] = -i\hbar \ln Z[K] - \int dx dy G(x, y) K(x, y), \quad (49)$$

where $K = K[G]$ satisfies Eq. (48). It then follows that

$$\frac{\partial \Gamma[G]}{\partial G(x, y)} = -K(x, y), \quad (50)$$

and thereby the minimum of Γ , given by $\partial \Gamma[G]/\partial G(x, y) = 0$, determines the value of $G(x, y)$ in the absence of an external source. This expression is useful because $\Gamma[G]$ can be written as a sum over all 2PI vacuum diagrams⁷⁸ and can therefore be calculated fairly easily in perturbation theory.

Although the 2PI formalism is in principle exact, in practice $\Gamma[G]$ must be calculated perturbatively. The lowest non-trivial contribution comes from two-loop diagrams. This two-loop approximation is equivalent to the Gaussian (Hartree) approximation.^{78,80} If we consider again the $O(N)$ scalar field theory (43), the equation of motion becomes

$$\partial_0^2 G(k) = - \left[k^2 + m^2 + (2 + N) \lambda \int \frac{dk'}{2\pi} G(k') \right] G(k), \quad (51)$$

where we have defined $G(k)$ as the Fourier transform of $G(x)$ given by $\langle \phi_i(x) \phi_j(y) \rangle = \delta_{ij} G(x - y)$. As in the linear approximation, we can then use Eq. (46) to estimate the number density of topological defects.

Because gauge fields lead to technical difficulties within this approach, it has only been applied to phase transitions in theories with global symmetries.⁸¹ The density of topological defects formed in an instantaneous quench was calculated by Antunes and Bettencourt,⁸² who also compared their results with the linear theory. Later, the Hartree approximation was also applied to non-instantaneous quenches in a two-dimensional theory with a global $O(2)$ symmetry by Bowick and Momen,⁸³ but they did not calculate the density of defects explicitly. In the case of an expanding universe, a proper numerical test for Zurek's predictions was carried out by Stephens *et al.*⁸⁴ who found the scaling laws $\hat{\xi} \propto \tau_Q^{0.35}$ for underdamped and $\hat{\xi} \propto \tau_Q^{0.28}$ for the overdamped cases, in a reasonable agreement with Zurek's predictions (25).

Although the 2PI formalism is sometimes called non-perturbative in the literature, it is only non-perturbative in the same sense as the calculation of the effective potential (15) using one-particle irreducible diagrams. This means that the critical exponents μ and ν in Eq. (24) produced by this approximation are not the true critical exponents of the system, but the perturbative ones. Therefore, the 2PI formalism at any finite loop order *cannot* give a correct description of the true dynamics of the phase transition. Nevertheless, it is still a non-trivial test for Zurek's predictions to check whether the results of the Hartree approximation agree with the predicted mean-field behaviour (25).

Being perturbative, the 2PI approximation is also insensitive to truly non-perturbative objects such as topological defects and therefore it cannot describe the formation of topological defects properly. This is obvious from Eq. (51), because the choice of the symmetry group $O(N)$ only affects the strength of the effective coupling between different modes, whereas in reality the dynamics at different N are very different: $N = 1$ gives rise to domain walls, $N = 2$ to vortices and $N = 3$ to monopoles. After all, the Hartree approximation is more or less equivalent to the leading term in the large- N approximation, and there are no topological defects in the large- N limit. Another flaw in this approximation is that it does not describe scattering of different Fourier modes properly, because each mode only interacts with the average of all the other modes.

The reason why Eq. (51) has such a simple form is that all the fundamental fields in the theory are related by a symmetry and therefore they all have the same two-point function. In more realistic theories, the equation of motion becomes more complicated, and the application of this formalism to gauge field theories is largely an unsolved problem. A further problem is that especially in gauge theories, even the equilibrium properties become non-perturbative near the transition and are therefore not correctly described by the 2PI effective action.

At two-loop level, there is no difference between classical and quantum mechanical time evolution. Because of this and the other problems mentioned above, it is essential to be able to go beyond the Gaussian approximation. At three-loop level,^{85,86} scattering of modes is taken into account, although it must still be assumed to be weak. In this approximation, some differences appear between classical and quantum dynamics, but the equations of motion still look very similar. Other ways of improving the Gaussian approximation have also been proposed.^{87,88,89}

6.3. *Classical approximation*

6.3.1. *Basics*

If we are willing to sacrifice the quantum mechanical nature of the system, it is relatively straightforward to study the dynamics in a fully non-perturbative way by simply solving numerically the classical equations of motion. In fact, this is believed to be a good approximation as long as the temperature is high enough, because the defect density and other physically relevant properties of the system after the transition are determined by the long-wavelength field modes, and they have high occupation numbers in thermal equilibrium.⁹⁰

A significant advantage of the classical approach over the 2PI formalism is that in the case of static equilibrium observables it is equivalent to dimensional reduction,^{27,28} *i.e.*, to an approach in which the full four-dimensional path integral is replaced by an effective three-dimensional one [see Eq. (14)]. Because the construction is free from infrared problems, it is believed that the effective theory describes the phase transition correctly. In particular, it belongs to the same uni-

versality class as the full quantum theory, and therefore the critical exponent ν in Eq. (24) has its true value. However, as discussed in Section 3, the universality arguments do not apply to the time dependence, and therefore the other critical exponent μ is not necessarily reproduced correctly. Nonetheless, the classical simulations provide a highly non-trivial, non-perturbative test for the mechanisms of defect formation.

The general strategy in classical simulations is to take an initial field configuration that is in thermal equilibrium and follow its time evolution by solving numerically the classical equations of motion. The thermal initial condition is typically prepared with a Monte Carlo algorithm of some type.^{91,92} Perhaps the most popular choice is to use Langevin dynamics,^{93,94} which means adding noise and damping terms to the equations of motion. In the case of an $O(N)$ symmetric scalar field theory, this means

$$\partial_0^2 \phi_i + \eta \partial_0 \phi_i - \vec{\nabla}^2 \phi_i - m^2 \phi_i - \lambda \phi_j \phi_j \phi_i = \zeta_i, \quad (52)$$

where the white noise term ζ satisfies

$$\langle \zeta_i(t, \vec{x}) \zeta_j(t', \vec{x}') \rangle = 2T\eta \delta_{ij} \delta(t - t') \delta^{(3)}(\vec{x} - \vec{x}'). \quad (53)$$

In the limit of infinite time, $t \rightarrow \infty$, and zero time step, the probability distribution of the field configurations approaches the canonical ensemble

$$p[\phi] \propto \exp(-H[\phi]/T), \quad (54)$$

where $H[\phi]$ is the Hamiltonian.

Another popular approach is the Metropolis algorithm,⁹⁵ which consists of making small random changes in the field configuration $\{\phi_i\} \rightarrow \{\phi'_i\}$ and calculating the corresponding changes ΔE in the total energy. If $\Delta E < 0$, the change is accepted, and if $\Delta E > 0$, it is accepted with probability $\exp(-\Delta E/T)$. When the number of these updates is large, the probability distribution of the field configurations again approaches the canonical ensemble. The Metropolis approach is generally more flexible than the Langevin approach, because the nature of the small random changes can be chosen to optimize the thermalization rate. In certain special cases, modifications of the Metropolis algorithm such as the heat bath algorithm,⁹⁶ in which one degree of freedom is brought in contact with a heat bath at a time, and hybrid Monte Carlo,⁹⁷ in which one uses the Hamiltonian time evolution to move the system around in the phase space, are more efficient.

In three dimensions, the energy density of a classical field theory in equilibrium is ultraviolet divergent, but this does not constitute a severe problem, because the space and time must be discretized in any case in order for the numerical solution to be possible, and this lattice cutoff $\Lambda = 1/a$ provides the necessary ultraviolet regularization. Nevertheless, these extra contributions should be renormalized, *i.e.*, the bare couplings used in the simulations must be chosen in such a way that they correspond to the desired infrared physics. In the limit of very fine lattices, $a \rightarrow 0$, we

can calculate perturbatively the counterterms that are sufficient for renormalizing all static equilibrium observables,^{98,99} but they leave some lattice spacing dependence in the time evolution.^{100,101} In particular, this discrepancy becomes worse in the continuum limit, and therefore we should not use too fine lattices.

It is quite common to keep phenomenological noise and damping terms in the equations of motion even during the time evolution of the system, in order to approximate the coupling to the other degrees of freedom. This time-dependent Ginzburg-Landau (TDGL) approach leads to a faster thermalization than the Hamiltonian equations of motion, but it does not change the nature of the dynamics qualitatively, because the interactions lead to thermalization in any case.

One advantage of classical simulations is that we can locate the defects directly in the field configurations and do not have to rely on the Halperin-Mazenko-Liu approximation (46). In a global U(1) theory, the lattice winding number is a straightforward analogue of the continuum one (6). For each link $(\vec{x}, \vec{x} + \hat{i})$, we define

$$\Delta\theta_{(\vec{x}, \vec{x} + \hat{i})} = [\theta(\vec{x} + \hat{i}) - \theta(\vec{x})]_\pi, \quad (55)$$

where the notation $[\dots]_\pi$ indicates that the difference is calculated in such a way that it always lies between $-\pi$ and π . This is equivalent to the geodesic rule. The winding number of a plaquette is then simply [cf. Eq. (6)]

$$N_{ij}(\vec{x}) = \frac{1}{2\pi} \left(\Delta\theta_{(\vec{x}, \vec{x} + \hat{i})} + \Delta\theta_{(\vec{x} + \hat{i}, \vec{x} + \hat{i} + \hat{j})} - \Delta\theta_{(\vec{x} + \hat{j}, \vec{x} + \hat{i} + \hat{j})} - \Delta\theta_{(\vec{x}, \vec{x} + \hat{j})} \right). \quad (56)$$

6.3.2. Global simulations

Antunes and Bettencourt⁸² compared the dynamics of the classical (1+1)-dimensional scalar field theory in an instantaneous quench with linear and Hartree approximations. Their results show that both approximations break down when the back-reaction becomes important, *i.e.*, when the order parameter reaches the minimum of the potential. Laguna and Zurek^{102,103} studied the formation of kinks in a linear quench in the same model in the overdamped case. They found a power law dependence $n \propto \hat{\xi}^{-1} \propto \tau_Q^{-0.28 \pm 0.02}$, which agrees with the mean-field Zurek prediction (25). Later,⁶¹ they investigated different cases that interpolate between the overdamped and underdamped dynamics and found power-law exponents ranging from -0.23 ± 0.01 (overdamped) to -0.33 ± 0.01 (underdamped). Moro and Lythe⁷⁶ also simulated the same system and confirmed their analytical prediction for the prefactor of the power law.

The reason why the above results are consistent with the mean-field expectations is that there is actually no phase transition at all in any (1+1)-dimensional classical model, and therefore no critical behaviour either. This also means that we cannot unambiguously measure the final defect density. In order to test the scenarios of defect formation properly, we have to go to higher dimensions.

Antunes *et al.*¹⁰⁴ studied the formation of vortices in a (3+1)-dimensional scalar field theory with a global O(2) symmetry. They used the TDGL approach and,

instead of varying the mass parameter m^2 , they changed the amplitude of the noise term, which effectively means changing the temperature of the heat bath to which the system is coupled. The final density of vortices per unit area had a power-law dependence on the quench rate $n \propto \hat{\xi}^{-2} \propto \tau_Q^{-0.4982 \pm 0.079}$. This is compatible with the overdamped mean-field prediction (25), although the classical simulation should experience the true critical behaviour with non-mean-field critical exponents. This is an indication that the freeze-out of the order parameter field took place before the system entered the critical region.

In their simulations within the same model, Bettencourt *et al.*¹⁰⁵ first carried out a linear temperature quench but then heated the system slightly above the critical temperature for a short time. They found that the original vortex network survives this period of symmetry restoration, which supports Zurek's idea that the defect distribution is determined by degrees of freedom whose dynamics are very slow near the transition even in the symmetric phase.

Stephens¹⁰⁶ used the TDGL approach to study the phase transition in the (2+1)-dimensional scalar field theory with a global O(3) symmetry. The topological defects in this model are textures, whose energy is independent of their size in the classical vacuum. Therefore not only the density but also the typical size of these objects is determined by the phase transition dynamics. The results show that the typical distance of the textures behaves as $L_{\text{sep}} \propto \tau_Q^{0.39 \pm 0.02}$ and the size as $L_w \propto \tau_Q^{0.46 \pm 0.04}$, whereas Zurek's prediction (25) for the freeze-out scale would have been $\hat{\xi} \propto \tau_Q^{0.25}$. However, these length scales evolve dynamically after the transition, which may explain the discrepancy.

6.3.3. Gauge field theories

One clear advantage of the classical approximation is that it can be easily applied to models with gauge symmetries. We shall discuss only the Abelian Higgs model here, but in principle similar techniques can and have been applied to non-Abelian theories.¹⁰⁷ The classical equation of motion for the gauge field is

$$D_\mu F^{\mu\nu} = j^\nu, \quad (57)$$

where $j^\nu = -2e\text{Im}\phi^*D^\nu\phi$ is the electric current. It is most convenient to use the temporal gauge $A_0 = 0$, because that simplifies the equation of motion into

$$\partial_0 \vec{E} = \vec{\nabla} \times \vec{\nabla} \times \vec{A} + \vec{j}, \quad (58)$$

where $\vec{E} = -\partial_0 \vec{A}$ is the electric field. However, in the temporal gauge we also obtain an extra constraint, which the field configurations must satisfy and which is nothing but the Gauss law

$$\vec{\nabla} \cdot \vec{E} = \rho, \quad (59)$$

where ρ is the electric charge.

The necessary discretization of this model is straightforward.¹⁰⁸ There are two alternative formulations, compact and non-compact, which correspond to gauge

groups $U(1)$ and \mathbb{R} , respectively. Because vortices are not absolutely stable in the compact formulation, we only consider the non-compact formulation here. The gauge field is described by a real-valued field $\alpha_\mu = aeA_\mu$, which is defined on links between lattice sites.

It is obvious that Eqs. (55) and (56) cannot be used in gauge field theories, since they are not gauge invariant. If the gauge is not fixed, the phase angles are totally random and uncorrelated, and therefore it is always trivially true that $N_{ij} = 1/3$.¹⁰⁹ The solution is to “relax the geodesic rule” by replacing the phase difference in Eq. (55) with its gauge-covariant counterpart^{110,109} [cf. Eq. (19)]

$$\Delta_{\text{cov}}\theta_{(\vec{x},\vec{x}+\hat{i})} = \left[\alpha_i(\vec{x}) + \theta(\vec{x} + \hat{i}) - \theta(\vec{x}) \right]_\pi - \alpha_i(\vec{x}). \quad (60)$$

When this is used in Eq. (56), the winding number becomes gauge invariant, and it is easy to see that it is always an integer. In fact, it is the natural lattice analogue of the continuum winding number N_W defined in Eq. (20).

6.3.4. Gauge simulations

Yates and Zurek⁶² investigated the phase transition in the (2+1)-dimensional Abelian Higgs model using the TDGL approach. They measured the number density of vortices after the transition, and found power laws $n \propto \hat{\xi}^{-2} \propto \tau_Q^{-0.44 \pm 0.10}$ for the overdamped case and $n \propto \hat{\xi}^{-2} \propto \tau_Q^{-0.60 \pm 0.07}$ for the underdamped case. These results agree with the mean-field prediction (25) based on the Kibble-Zurek mechanism. The values they used for the gauge coupling constant and temperature, $e = 0.5$ and $T = 0.01$, were so low that the flux trapping mechanism (33) does not have significant effects. Indeed, the typical flux through their whole 512^2 lattice is merely $\Phi \approx 4\Phi_0$ according to Eq. (31). They also used Eq. (55) to define the winding number, but again because of the low temperature, this did not affect the results.

The (2+1)-dimensional Abelian Higgs model was also studied by Ibaceta and Calzetta,¹¹¹ who used the overdamped TDGL approach. Because they used an instantaneous quench, they were not able to test the predictions for the defect density. On the other hand, their aim was to test the applicability of the linear approximation, and they found that although it eventually breaks down, it agrees very well at early times. This is presumably partly because they used Gaussian initial conditions for the Higgs field rather than thermal ones. In their initial conditions, the gauge field vanished everywhere, so they could not have observed the flux trapping mechanism in any case. Furthermore, they used Eq. (55) as the definition for the winding number.

The only (3+1)-dimensional simulations in a gauge field theory so far have been carried out by Hindmarsh and Rajantie.^{14,65} In Ref. 14, they used the classical approximation without damping and noise terms. In their lattice, one of the dimensions was shorter than the other two, in order to stabilize vortices that wind around that dimension so that they can be counted. They prepared the initial configuration

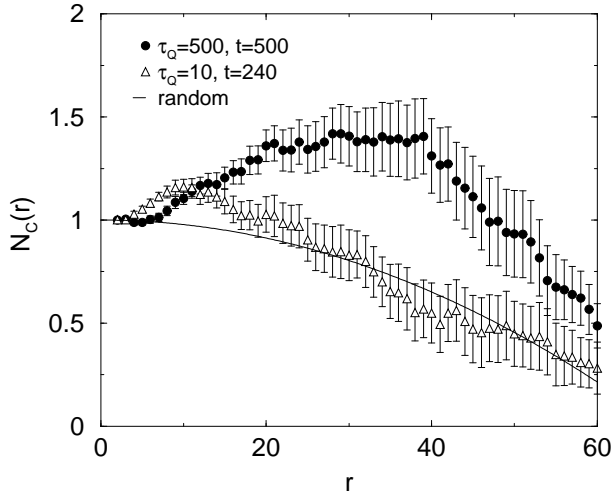


Figure 4: The correlation function $N_C(r)$ [see Eq. (39)] measured by Hindmarsh and Rajantie¹⁴ in two quenches with different τ_Q . The solid line illustrates the effect of the finite system size by showing $N_C(r)$ for a random distribution of vortices and antivortices. In both runs, $N_C(r)$ is above this curve, which supports the flux trapping scenario, as discussed in Section 5.3 (see also Fig. 3). (From Ref. 14.)

using a hybrid Monte Carlo algorithm,⁹² and used a time-varying mass term in their simulations. They used the gauge-invariant definition (60) for the winding number to locate the defects in the final state, and found the power-law $n \propto \tau_Q^{-0.250 \pm 0.013}$ when the short dimension was 5 in lattice units, and $n \propto \tau_Q^{-0.274 \pm 0.039}$ when it was 20. These results disagree strongly with Zurek's prediction (25), which is $n \propto \tau_Q^{-2/3}$. On the other hand, they can be explained in terms of the flux trapping mechanism.

From the viewpoint of vortex dynamics, the system they studied was effectively two-dimensional and therefore the relevant theoretical predictions correspond to $D = 2$ in Eq. (33), *i.e.*,¹⁴

$$n \approx \frac{e}{2\pi} \frac{T^{1/2}}{L_z^{1/2} \hat{\xi}}, \quad (61)$$

where L_z is the extent of the system in the short dimension. This predicted dependence on L_z was confirmed in the simulations.¹⁴ Note, however, that using Eqs. (37) and (61), we expect $n \propto \tau_Q^{-0.2}$. This discrepancy is explained by the failure of the classical approximation to describe the time evolution of the quantum theory correctly. In particular, Landau damping (35) is very sensitive to the quantum mechanical ultraviolet modes, and in the classical theory, it actually behaves more like⁶⁵ $\gamma_L(k) \propto k^{2.1}$. Substituting this into Eqs. (34) and (61), we find $n \propto \tau_Q^{-0.24}$, in a fair agreement with the measurements.

As discussed in Section 5.3, the flux trapping mechanism also predicts a characteristic spatial distribution for the vortices. Hindmarsh and Rajantie¹⁴ studied that

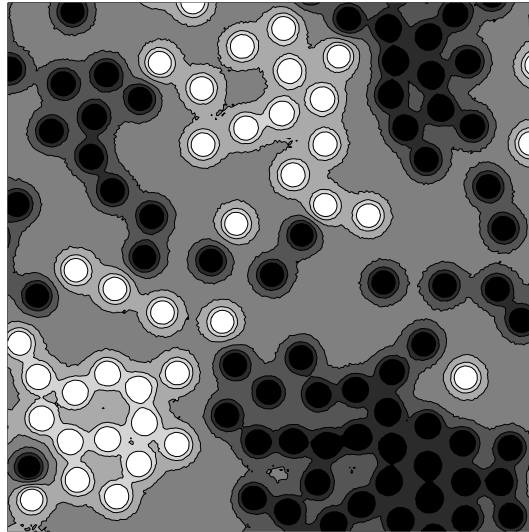


Figure 5: An example of the spatial vortex distribution after a phase transition in the simulations of Stephens *et al.*⁶³ White and black circles correspond to vortices and antivortices, respectively. The plot shows clearly the clustering of vortices discussed in Section 5.3. (From Ref. 63, kindly supplied by G. Stephens.)

in their simulations by measuring the function $N_C(r)$ [see Eq. (39)]. Their results for two different quench rates are shown in Fig. 4, and they display a clear positive correlation at short distances, as predicted by the flux trapping mechanism.

More recently, Stephens *et al.*⁶³ studied instantaneous phase transitions in the (2+1)-dimensional Abelian Higgs model using overdamped TDGL simulations. They found very strong clustering of vortices, as shown in Fig. 5, in agreement with the discussion in Section 5.3. They also measured the dependence of the vortex density on the gauge coupling and temperature, and found the relation $n \approx CeT^{1/2}$, where C is a constant. This confirms the prediction (33) of the flux trapping scenario.

People have also studied inhomogeneous setups with the motivation that they might be more relevant for actual experimental phase transitions.⁵⁷ Dziarmaga *et al.*¹¹² used the TDGL approach in a global theory in (1+1) dimensions to study a phase transition which starts from one end of the system and propagates to the other. They found significant suppression of defect density. Aranson *et al.*^{113,114} have used overdamped TDGL simulations to study a global (3+1)-dimensional U(1) theory in an inhomogeneous case, in which the system was initially heated up locally at a single point.

6.4. Hard-thermal-loop improvement

When discussing the classical approximation in Section 6.3, we implicitly assumed that the classical theory had the same Lagrangian as the full quantum theory it was

supposed to approximate. However, Bodeker *et al.*^{100,101} showed that this leads to wrong dynamics, although it reproduces the static equilibrium properties correctly, once simple renormalization counterterms are included.

The reason for this failure is that the classical approximation is only valid for long-wavelength modes. Therefore, the classical theory must be interpreted as an effective theory in the Wilsonian sense, and in principle, its Lagrangian should contain all the terms that are compatible with the symmetries of the system. In vacuum, these terms are strongly constrained by the Lorentz invariance, but at a non-zero temperature, Lorentz invariance is broken by the rest frame of the thermal background. Therefore many more terms are allowed in the effective Lagrangian and restricting it to its original form is not justified.

Fortunately, the difference between the quantum and classical theories appears only at very high momenta, and these ultraviolet degrees of freedom are perturbative. Therefore we can calculate the necessary corrections to the classical Lagrangian perturbatively. In a global scalar theory, we only obtain a simple mass counterterm, but in gauge field theories, the correction is a complicated non-local object.¹¹⁵ In the Abelian Higgs model, this *hard-thermal-loop* improved effective Lagrangian is¹¹⁶

$$\begin{aligned} \mathcal{L}_{\text{HTL}} = & -\frac{1}{4}F_{\mu\nu}F^{\mu\nu} - \frac{1}{4}m_D^2 \int \frac{d\Omega}{4\pi} F^{\mu\alpha} \frac{v_\alpha v^\beta}{(v \cdot \partial)^2} F_{\mu\beta} \\ & + |D_\mu \phi|^2 - m_T^2 |\phi|^2 - \lambda |\phi|^4, \end{aligned} \quad (62)$$

where $m_T^2 = m^2 + (e^2/4 + \lambda/3)T^2$, and the integration is taken over the unit sphere of velocities $v = (1, \vec{v})$, $\vec{v}^2 = 1$. The Debye screening mass has the value $m_D^2 = \frac{1}{3}e^2 T^2$. We have here ignored a similar, non-physical, contribution that arises from ultraviolet lattice modes, and which should in principle be subtracted.¹¹⁷ Therefore we must assume that the lattice spacing is long enough, $a \gg T^{-1}$, so that this contribution is negligible. Because the perturbative calculation that gave Eq. (62) involved only hard, ultraviolet modes, it is believed to be reliable as long as the coupling constants are small.¹¹⁸

In principle, we can simulate the dynamics of the theory by solving numerically the equations of motion derived from Eq. (62). However, because the extra term is non-local this requires keeping all the previous time steps in the memory. Instead, it is much more convenient to introduce extra degrees of freedom, which have local interactions, and which reproduce the same effective term. There are different ways of doing this: The extra degrees of freedom can either be point particles¹¹⁹ or fields.^{120,118,121}

The HTL approach has been used to study equilibrium quantities such as the rate of baryon number violation in the symmetric phase of the electroweak theory.^{119,121} Similarly, Hindmarsh and Rajantie⁶⁵ used it in the Abelian Higgs model to measure the real-time correlator of the magnetic field at the transition point. They found that within the range of wavelengths they studied, the time scale that dominates the dynamics of the long-wavelength magnetic fields is determined by the Landau damping rate γ_L and that at intermediate wavelengths it agrees with the pertur-

bative result (35). Because γ_L is very sensitive to quantum effects — they also measured the rate without the HTL correction and obtained a very different result — this is a very strong indication that the HTL approach really approximates the full quantum dynamics well. Nonetheless, because the approximation ignores the scattering of hard modes, it eventually breaks down at very long wavelengths, $k \lesssim e^4 T$, and very long times.

The HTL approximation can also be used in non-equilibrium settings provided that the ultraviolet modes are still in equilibrium, which is the case in thermal phase transitions.¹¹⁸ Hindmarsh and Rajantie⁶⁵ used this approach to study vortex formation in the phase transition of the Abelian Higgs model, and found $n \propto \tau_Q^{-0.201 \pm 0.015}$. This differs from the prediction of the Kibble-Zurek mechanism (25) which is $n \propto \hat{\xi}^{-2} \propto \tau_Q^{-0.5 \dots -0.66}$, but agrees very well with the flux trapping predictions (37) and (61).

7. Experiments

The similarity of defect formation in condensed matter systems and cosmology was already noted by Zeldovich *et al.*⁴³ and Kibble,^{1,59} but the first concrete proposal of utilizing this correspondence to test the cosmological scenarios in experiments was made by Zurek.^{5,60} He suggested an experiment in which a pressure quench would be used to cause a phase transition in ${}^4\text{He}$ and which was later carried out by Hendry *et al.*¹⁰

Later on, other condensed matter systems have been used to study defect formation as well. Most of them, liquid crystals,^{8,9} ${}^4\text{He}$ ^{10,13} and ${}^3\text{He}$ -B^{11,12} are systems with global symmetries, and therefore the applicable theoretical scenario is the Kibble-Zurek scenario. The same applies to recent studies of non-linear optical systems¹²² and convection in fluids,¹²³ as well as to the proposed experiments with atomic Bose-Einstein condensates.¹²⁴

The only exception are superconductors.¹⁹ The order parameter, the Cooper pair, is electrically charged, and therefore the symmetry that is broken is a local symmetry. This means that the flux trapping mechanism should form vortices in addition to the Kibble-Zurek mechanism. So far, only two superconductor experiments have been carried out,^{125,126} and they haven't been able to give conclusive results, but the rapid progress in experimental techniques in the recent years suggests that more detailed experiments will soon be possible.

7.1. Liquid crystals

Liquid crystals¹²⁷ are perhaps the simplest condensed matter systems in which formation of topological defects can be studied. The phase transition between isotropic and nematic phases takes place near the room temperature, and the defects can be seen with an optical microscope. A disadvantage of liquid crystals is that the transition is of first order and therefore it cannot really probe the Kibble-Zurek mechanism, which applies to continuous phase transitions.

A nematic liquid crystal consists of rod-like molecules, whose orientation acts as the order parameter. It is an unoriented three-vector and is commonly denoted by \vec{n} . The vacuum manifold is S^2/\mathbb{Z}_2 and has non-trivial first, second and third homotopy groups. Therefore, the system has three types of topological defects: vortex lines (strings), monopoles and textures.

The first experimental study of defect formation was carried out by Chuang *et al.*⁸ and concentrated mainly on the dynamics of the string network after the transition from the isotropic to the nematic phase. Bowick *et al.*⁹ paid more attention to the formation of the defects, and carried out a quantitative comparison with the Kibble mechanism. Because the phase transition is of first order, the number density of vortex lines in the nematic phase should be given by Eq. (18). They counted the number of bubbles, compared it with the number of vortices and found a good agreement with the theoretical prediction.

As discussed in Section 5.3, the spatial distribution of defects is a very convenient way to test the mechanisms for defect formation. Because the symmetry broken in the isotropic-nematic phase transition is global, the relevant theoretical scenario is the Kibble mechanism, and it predicts strong negative correlations between defects. These correlations were studied experimentally by Digal *et al.*⁶⁷ They measured the net number of vortices $N_W(A)$ through a loop of area A . On average, this is obviously zero, because vortices of either sign have the same probability, but the width σ of the distribution depends on the correlations of the vortices. Digal *et al.* assumed a power-law behaviour

$$\sigma = CN^\nu, \quad (63)$$

where C and ν are free parameters. They used the total number of vortices N inside the loop instead of A , because it separates the effects of the vortex correlations from the relation between N and A .

The Kibble mechanism predicts $\nu = 1/4$, but if the vortices were randomly distributed, the exponent would be $\nu = 1/2$. The measured value for the exponent was $\nu = 0.26 \pm 0.11$, in a good agreement with the Kibble mechanism. Moreover, Digal *et al.* measured the value of the prefactor $C = 0.76 \pm 0.21$, which also agrees well with the theoretical prediction $C \approx 0.71$, calculated using the simplifying assumption that the bubble nucleation sites form a square lattice.

7.2. Superfluids

At low enough temperatures, helium becomes a superfluid,¹⁹ and this transition can also be described as a spontaneous breakdown of a global symmetry. It has the advantage over liquid crystals that superfluidity is a quantum phenomenon, and therefore the experiments can really probe the behaviour of a quantum field theory rather than a classical one.

In the ${}^4\text{He}$ isotope, the phase transition to the superfluid phase takes place at the critical temperature $T_\lambda \approx 2.18$ K. In the Ginzburg-Pitaevskii¹²⁸ picture of the transition, the order parameter ψ is the quantum mechanical wave function of the

^4He atoms. In practice, ψ is a complex scalar field, and the theory is invariant under global $U(1)$ transformations. In the superfluid phase, the ^4He atoms form a Bose condensate, which is signalled by a non-zero vacuum expectation value of ψ . This breaks the $U(1)$ symmetry, and as discussed in Section 2, leads to the existence of vortex line solutions.

Vortex formation in a ^4He phase transition was first studied experimentally by Hendry *et al.*¹⁰ They had a small volume of ^4He in a container at a temperature slightly above T_λ , and instead of cooling the system, they expanded the container rapidly so that the pressure decreased. This increases T_λ , and therefore the system underwent a phase transition into the superfluid phase. They counted the vortices formed in the transition by measuring the attenuation of the second sound in the liquid after the transition. The results show that vortices were indeed formed in the transition, but this was later attributed to hydrodynamic effects that arise from non-idealities in the experimental setup rather than to the Kibble-Zurek mechanism.¹²⁹

A more careful study was carried out later by Dodd *et al.*^{13,130} who eliminated the most significant sources for hydrodynamic vortex formation. Surprisingly, they did not find any evidence for vortex formation in the transition. They suggested that the vortices may have decayed faster than expected. This idea was made more precise by Karra and Rivers,⁷⁴ who argued that the Ginzburg temperature T_G [see Eq. (22)], above which thermal fluctuations are still able to restore the symmetry within a correlated region, is well below T_λ in ^4He , and in fact, the final state was still above T_G in the experiment. Therefore, the vortices never became well defined classical objects and were washed out by thermal fluctuations before being observed.

The other helium isotope ^3He also displays superfluidity at low temperatures,¹⁹ but many details are very different. Because ^3He atoms are fermions, they can only condensate if they form bosonic Cooper pairs. Therefore, superfluidity needs millikelvin temperatures, much lower than in ^4He . Furthermore, the Cooper pairs may have a non-trivial spin \mathbf{S} and angular momentum \mathbf{L} , which means that the order parameter is more complicated than simply a complex scalar field. Therefore, there are different superfluid phases: the A phase, which is only present in a narrow range of temperatures and under high pressures or if a strong external magnetic field is applied, and the B phase. In an external magnetic field, a third superfluid phase, known as the A1 phase, is also possible.

In all the existing experiments, the transitions have been between the normal and the B phase, and therefore we shall only concentrate on that. In the B phase, the total angular momentum $\mathbf{J} = \mathbf{L} + \mathbf{S}$ vanishes. The symmetry breaking structure is¹⁹

$$\text{SO}(3)_{\mathbf{L}} \times \text{SO}(3)_{\mathbf{S}} \times U(1)_\phi \rightarrow \text{SO}(3)_{\mathbf{L}+\mathbf{S}}. \quad (64)$$

This allows two different types of vortices, oriented *mass vortices* and unoriented *spin vortices*.¹³¹ The latter ones are bound to soliton sheets and are therefore unstable.

Vortex formation in ^3He has been studied in two experiments.^{11,12} They both used external neutron sources to heat up the system locally. When a neutron hits

a ${}^3\text{He}$ nucleus, it may be captured in the reaction



This releases 764 keV of energy, which heats up a “hot spot” of radius $\approx 30 \mu\text{m}$, and inside this hot spot the symmetry is locally restored. The hot spot cools rapidly in about 1 μs , and undergoes a phase transition back to the superfluid phase. According to the Kibble-Zurek scenario, a tangle of vortices is formed in this process.

In the Helsinki experiment by Ruutu *et al.*¹² the cryostat that contained the helium was rotating with a velocity lower than the critical velocity of the superfluid. This rotation expands those vortex loops that are larger than a certain critical size. Eventually, they straighten out and move to the centre of the container. Using NMR spectroscopy, Ruutu *et al.* were able to count the vortices one by one and thereby obtained a very precise measurement for the number of vortices formed in the transition.

In the Grenoble experiment carried out by Bäuerle *et al.*¹¹ the number of vortices formed in the transition was inferred using a vibrating superconducting wire, which measures the amount of heat deposited in the liquid very accurately. If vortices are formed, this amount is less than the total 764 keV released in the neutron capture event, because some of the energy is stored in the vortices. The experiment was carried out at a temperature well below T_c so that the lifetime of the vortices was much longer than the time needed for the measurement.

In both ${}^3\text{He}$ experiments, the measured number of vortices was in a reasonable agreement with the prediction of the Kibble-Zurek mechanism. In experiments of this type, the quench timescale τ_Q is not a free parameter, because it is determined by the equilibration rate of the system after a neutron capture event, and therefore it is not possible to study the dependence of the vortex number on τ_Q . Nevertheless the results show beyond doubt that vortices are formed in the transition, in contrast to ${}^4\text{He}$, which may be explained by the fact that in ${}^3\text{He}$, T_G is very close to T_c .⁷⁴

In the above experiments, the observed vortices were mass vortices, but more recently, Eltsov *et al.*¹³² have also reported an observation of composite *spin-mass vortices* after a phase transition to the B phase.

Another type of a superfluid experiment was also suggested by Zurek.⁵ He pointed out that if the superfluid container is an annulus instead of a cylinder, the “vortices” that are formed in the transition pass through the hole. Because their cores are outside the superfluid, they cost very little energy and are therefore very stable. They can be detected as a non-zero angular velocity of the superfluid around the annulus. However, this experiment has not been carried out yet.

7.3. Other global systems

The liquid crystal and superfluid experiments were not able to measure the dependence of the vortex number on τ_Q and therefore they could not test the Kibble-Zurek

mechanism quantitatively. However, there have recently been reports of other studies in which this has been done.^{122,123}

The first such experiment was carried out by Ducci *et al.*¹²² in a non-linear optical system. They studied a liquid crystal light valve illuminated by a laser beam and inserted in a feedback loop. When the intensity of the incident light exceeds a threshold value, an intensity patterns of standing rolls forms. The authors changed the intensity of the light at a finite rate characterized by τ_Q , recorded the intensity pattern and counted the defects. They found a power-law dependence $n \propto \tau_Q^{-0.50 \pm 0.04}$, in a very good agreement with Zurek's prediction (25).

Casado *et al.*¹²³ studied the breaking of a global symmetry in the Bénard-Marangoni conduction-convection transition. They heated up the bottom of a cylindrical container with a layer of silicone oil in it. Below a certain critical temperature T_c , the fluid is in a homogeneous conduction state, but above T_c , the symmetry is broken by a hexagonal array of convection lines where hot fluid flows upwards. Casado *et al.* captured the image with a CCD camera and located the defects in the array structure. They used different rates of increasing the temperature at the bottom of the container, characterized by the quench time scale τ_Q . The number of defects had a power-law dependence on τ_Q , with exponent ranging from -0.45 to -0.25 depending on the viscosity of the fluid.

7.4. Superconductors

All the experiments discussed above are systems with broken global symmetries, whereas local gauge symmetries are more relevant for particle physics and cosmology. Therefore, it has been appreciated for a long time^{51,64,133} that defect formation should also be studied experimentally in type-II superconductors.

In superconductors,¹⁹ the order parameter is a scalar field ψ , which describes the Cooper pairs. The field is charged under the U(1) gauge group of electrodynamics, because the Cooper pairs have an electric charge of $-2e$. In the superconducting phase, the Cooper pairs condense, and this leads to the Meissner effect. The equilibrium properties of superconductors near the phase transition are described by the Ginzburg-Landau theory, which is very similar to the Abelian Higgs model (7). Although the details of the dynamics are presumably quite different, the considerations that led to the flux trapping mechanism (see Section 5.2) are still valid, and therefore the mechanism can be tested in superconductor experiments.

In principle, the required experimental setup is relatively simple. A superconducting film is cooled through the phase transition from the normal phase into the superconducting phase, and the vortices formed in the transition are detected by measuring their magnetic field.

In practice, there are many difficulties in this kind of an experiment. A slightly simpler setup⁶⁴ involves a superconducting loop, which is quenched through the phase transition. In this kind of a system, the “vortices” show up as a non-zero magnetic flux through the loop. The Kibble-Zurek mechanism predicts $N_{\text{KZ}} \approx (L/\hat{\xi})^{1/2}$ flux quanta, where L is the circumference of the loop, and the magnetic field trapped

according to the flux trapping mechanism consists of $N_{\text{trap}} \approx (e^2 TL)^{1/2}$ flux quanta, independently of the quench rate, provided that $\hat{\xi} < L$.

An experiment that was essentially like this was carried out by Carmi *et al.*¹²⁶ They used a 1 cm^2 loop of $\text{YBa}_2\text{Cu}_3\text{O}_{7-\delta}$ superconductor built from 214 Josephson junctions. A light beam was used to heat the loop above $T_c \approx 90 \text{ K}$, and when the light was switched off, a thermal link to a heat bath cooled the loop through the phase transition. The cooling rates varied from 0.3 to 20 K/s. They measured the flux through the loop after the transition using a superconducting quantum interference device (SQUID) magnetometer placed at a distance of 1 mm from the loop, and found that its was zero on average and the distribution had a standard deviation of $\sigma_{\text{exp}} = 7.4 \pm 0.7$ flux quanta, independently of the cooling rate.

In this setup, the Kibble-Zurek mechanism predicts that the phase of the order parameter is independent in each of the $N = 214$ segments, and therefore the resulting standard deviation should be roughly $\sigma_{\text{KZ}} = C\sqrt{N} \approx 14.6C$, where C is some constant of order one. This result agrees well with the observations, and is indeed independent of the quench rate, as observed. The contribution predicted by the flux trapping mechanism is¹⁴ $\sigma_{\text{trap}} \approx 4$ flux quanta, and therefore the experiment cannot really distinguish between the two mechanisms.

What simplifies the superconductor loop experiment is that the “vortices” are formed outside the superconductor itself. This, however, also means that the experiment does not really probe the dynamics inside the superconductor, and indeed in the experiment by Carmi *et al.*¹²⁶ the numbers of vortices predicted by the Kibble-Zurek and flux trapping mechanisms are both independent of the quench rate.

Carmi and Polturak¹²⁵ also carried out a similar experiment with a superconducting $\text{YBa}_2\text{Cu}_3\text{O}_{7-\delta}$ film of size 1 cm^2 . Again, they heated the film with light, switched the light off and measured the resulting magnetic flux through the film when the system had reached the superconducting phase. They estimated that the sensitivity of their measurement was around 20 flux quanta, and they could not find any evidence of vortices being formed. They compared this with their own theoretical estimate, which was around 10000, and concluded that there is a clear discrepancy. However, their theoretical picture was rather different from the Kibble-Zurek or flux trapping scenarios, which predict much fewer vortices, of order 100 and 1, respectively.^{134,14}

In the film experiment,¹²⁵ the Kibble-Zurek prediction depends on the quench rate, so one could test the scenario by measuring this dependence. However, the prediction also depends on details of the dynamics that have not yet been properly understood, and therefore it is not a very robust test. Moreover, the flux trapping scenario becomes slightly more complicated because the magnetic field extends outside the two-dimensional film.^{14,66} For this reason, simple two-dimensional simulations such as those in Ref. 63 do not describe the transition correctly.

On the other hand, as pointed out in Section 5.3, the two scenarios predict very characteristic correlations between the produced vortices, and therefore a measurement of the spatial vortex distribution is the best way of distinguishing between the

mechanisms. Unfortunately, this was not possible in the experiments carried out by Carmi *et al.*^{125,126} because they only measured the total magnetic flux.

In order to measure the spatial vortex distribution, one has to face several technical problems. First of all, one has to be able to identify individual vortices, which means a sensitivity to fluxes at a level well below one flux quantum. Secondly, the spatial resolution must be high enough so that one can see the correlations, and finally, the measurement must be fast enough so that the vortices do not have time to annihilate. There are several different methods available,¹³⁵ all of which have their strengths and weaknesses. Scanning SQUID microscopy has a very high sensitivity and reasonably high spatial resolution, but the measurements take minutes. Real-time imaging at video rate with a sensitivity to a single flux quantum has been achieved using Lorentz microscopy¹³⁶ and magneto-optical imaging.¹³⁷

The dynamics of the vortices after the transition are complicated by the impurities in the superconductor film, which tend to pin vortices to them. This effect can also be used to simplify the measurement by constructing a regular array of pinning sites from submicron holes (antidots).¹³⁸ When the vortices get pinned to the antidots, their spatial distribution is stabilized and can be measured with slower techniques such as scanning SQUID microscopy and scanning Hall probe microscopy.

A further type of an experiment has been proposed by Kavoussanaki *et al.*¹³⁹ who suggested using an annular Josephson junction consisting of two superconducting loops separated by a thin layer of insulator. This system is described by the sine-Gordon theory, whose field is the phase angle difference of the order parameter fields in the two loops. A soliton of the sine-Gordon model corresponds to a case with different magnetic fluxes through the two loops, and the Kibble-Zurek mechanism predicts that these solitons are formed in the transition.

8. Conclusions

In this article, we have discussed the formation of topological defects in field theory phase transitions. In particular, we have concentrated on the differences between gauge field theories and theories with global symmetries.

While the Kibble-Zurek scenario,^{1,5} which applies to theories with global symmetries, has been around for decades and has been tested both in numerical simulations and in various condensed matter experiments, the same phenomenon in gauge field theories has remained poorly understood until very recently. However, in the last couple of years, the role of magnetic field has been clarified and a theoretical picture of defect formation based on the trapping of magnetic flux has emerged.¹⁴ Both the Kibble-Zurek and the flux trapping mechanisms are based on a freeze-out of long-wavelength modes that are too slow to adapt to the change of the external parameters. It is noteworthy that very similar phenomena are expected to take place in heavy-ion collisions.^{3,4}

We have reviewed the basic predictions of the Kibble-Zurek and flux trapping scenarios. The numbers of vortices formed by these two mechanisms depend on

the temperature, the rate of the phase transition and other parameters in different ways. Furthermore, the mechanisms lead to very different spatial distributions of vortices: While the Kibble-Zurek mechanism predicts negative correlations between the defects, the correlations are positive in the flux trapping scenario. This means that flux trapping typically forms clusters of vortices with equal sign, and depending on the parameters, these clusters can be large.

These predictions have been confirmed in numerical simulations, but they can also be tested in superconductor experiments, which are made possible by the recent developments in experimental techniques. This has been demonstrated in the recent pioneering experiments,^{125,126} and there is little doubt that proper experimental tests will be carried out in the near future.

These experiments will provide us with valuable information about the non-equilibrium dynamics of gauge field theories during phase transitions. This is extremely important for particle physics and cosmology, as well, because once the behaviour in a simpler system such as a superconductor is understood, similar theoretical techniques can be applied to heavy ion collisions and cosmological phase transitions.

Acknowledgements

The author wishes to thank Gert Aarts, Nuno Antunes, Dan Cormier, Anne-Christine Davis, Tom Girard, Mark Hindmarsh, Tom Kibble, Ray Rivers, Greg Stephens, Neil Turok and Wojciech Zurek for useful discussions and correspondence. This work was supported by PPARC, the ESF programme Cosmology in the Laboratory (COSLAB) and the UK Thermal Field Theory network.

References

1. T. W. B. Kibble, J. Phys. A **9** (1976) 1387.
2. A. Vilenkin and E.P.S. Shellard, *Cosmic Strings and Other Topological Defects* (Cambridge University Press, Cambridge, 1994).
3. B. Berdnikov and K. Rajagopal, Phys. Rev. D **61** (2000) 105017 [hep-ph/9912274].
4. D. Boyanovsky, H. J. de Vega and M. Simionato, Phys. Rev. D **63** (2001) 045007 [hep-ph/0004159].
5. W. H. Zurek, Nature **317** (1985) 505.
6. J. Zinn-Justin, *Quantum Field Theory and Critical Phenomena* (Clarendon Press, Oxford, 1989).
7. M. Stephanov, K. Rajagopal and E. Shuryak, Phys. Rev. Lett. **81** (1998) 4816 [hep-ph/9806219].
8. I. Chuang, R. Durrer, N. Turok and B. Yurke, Science **251** (1991) 1336.
9. M. J. Bowick, L. Chandar, E. A. Schiff and A. M. Srivastava, Science **263** (1994) 943 [hep-ph/9208233].
10. P. C. Hendry *et al.*, Nature **368** (1995) 315.
11. C. Bäuerle *et al.*, Nature **382** (1996) 332.
12. V. M. Ruutu *et al.*, Nature **382** (1996) 334 [cond-mat/9512117].
13. M. E. Dodd *et al.*, Phys. Rev. Lett. **81** (1998) 3703 [cond-mat/9808117].
14. M. Hindmarsh and A. Rajantie, Phys. Rev. Lett. **85** (2000) 4660 [cond-mat/0007361].
15. M. B. Hindmarsh and T. W. B. Kibble, Rept. Prog. Phys. **58** (1995) 477 [hep-

ph/9411342].

16. J. Magueijo and R. H. Brandenberger, in *Large Scale Structure Formation*, edited by R. Mansouri and R. H. Brandenberger (Kluwer, Dordrecht, 2000) [astro-ph/0002030].
17. H. B. Nielsen and P. Olesen, *Nucl. Phys. B* **61** (1973) 45.
18. L. Jacobs and C. Rebbi, *Phys. Rev. B* **19** (1979) 4486.
19. D. R. Tilley and J. Tilley, *Superfluidity and Superconductivity* (IOP, Bristol, 1990).
20. E. B. Bogomolny, *Sov. J. Nucl. Phys.* **24** (1976) 449 [*Yad. Fiz.* **24** (1976) 861].
21. G. 't Hooft, *Nucl. Phys. B* **79** (1974) 276.
22. A. M. Polyakov, *JETP Lett.* **20** (1974) 194 [*Pisma Zh. Eksp. Teor. Fiz.* **20** (1974) 430].
23. J. P. Preskill, *Phys. Rev. Lett.* **43** (1979) 1365.
24. A. H. Guth, *Phys. Rev. D* **23** (1981) 347.
25. J. I. Kapusta, *Finite-Temperature Field Theory* (Cambridge University Press, Cambridge, 1989).
26. D. J. Gross, R. D. Pisarski and L. G. Yaffe, *Rev. Mod. Phys.* **53** (1981) 43.
27. P. Ginsparg, *Nucl. Phys. B* **170** (1980) 388.
28. K. Kajantie, M. Laine, K. Rummukainen and M. Shaposhnikov, *Nucl. Phys. B* **458** (1996) 90 [hep-ph/9508379].
29. K. Kajantie, M. Laine, K. Rummukainen and M. Shaposhnikov, *Nucl. Phys. B* **493** (1997) 413 [hep-lat/9612006].
30. R. Jackiw, *Phys. Rev. D* **9** (1974) 1686.
31. S. Elitzur, *Phys. Rev. D* **12** (1975) 3978.
32. S. Coleman and E. Weinberg, *Phys. Rev. D* **7** (1973) 1888.
33. B. I. Halperin, T. C. Lubensky and S.-K. Ma, *Phys. Rev. Lett.* **32** (1974) 292.
34. E. Fradkin and S. H. Shenker, *Phys. Rev. D* **19** (1979) 3682.
35. H. Kleinert, *Lett. Nuovo Cim.* **35** (1982) 405.
36. A. Kovner, B. Rosenstein and D. Eliezer, *Nucl. Phys. B* **350** (1991) 325.
37. J. S. Langer, *Annals Phys.* **41** (1967) 108.
38. J. S. Langer, *Annals Phys.* **54** (1969) 258.
39. S. Coleman, *Phys. Rev. D* **15** (1977) 2929 [Erratum-*ibid. D* **16** (1977) 1248].
40. G. D. Moore and K. Rummukainen, *Phys. Rev. D* **63** (2001) 045002 [hep-ph/0009132].
41. H. Kurki-Suonio and M. Laine, *Phys. Rev. Lett.* **77** (1996) 3951 [hep-ph/9607382].
42. J. Ignatius, K. Kajantie, H. Kurki-Suonio and M. Laine, *Phys. Rev. D* **49** (1994) 3854 [astro-ph/9309059].
43. Y. B. Zeldovich, I. Y. Kobzarev and L. B. Okun, *Zh. Eksp. Teor. Fiz.* **67** (1974) 3 [*Sov. Phys. JETP* **40** (1974) 1].
44. T. Vachaspati and A. Vilenkin, *Phys. Rev. D* **30** (1984) 2036.
45. T. Prokopec, *Phys. Lett. B* **262** (1991) 215.
46. R. J. Scherrer and J. A. Frieman, *Phys. Rev. D* **33** (1986) 3556.
47. J. Borrill, T. W. B. Kibble, T. Vachaspati and A. Vilenkin, *Phys. Rev. D* **52** (1995) 1934 [hep-ph/9503223].
48. A. A. de Laix and T. Vachaspati, *Phys. Rev. D* **59** (1999) 045017 [hep-ph/9802423].
49. A. Melfo and L. Perivolaropoulos, *Phys. Rev. D* **52** (1995) 992 [hep-ph/9501284].
50. A. Ferrera and A. Melfo, *Phys. Rev. D* **53** (1996) 6852 [hep-ph/9512290].
51. S. Rudaz and A. Mohan Srivastava, *Mod. Phys. Lett. A* **8** (1993) 1443 [hep-ph/9212279].
52. M. Hindmarsh, A. Davis and R. Brandenberger, *Phys. Rev. D* **49** (1994) 1944 [hep-ph/9307203].
53. T. W. B. Kibble and A. Vilenkin, *Phys. Rev. D* **52** (1995) 679 [hep-ph/9501266].
54. J. M. Kosterlitz and D. J. Thouless, *J. Phys. C* **6** (1973) 1181.
55. N. C. Mermin and H. Wagner, *Phys. Rev. Lett.* **17** (1966) 1133.
56. S. Coleman, *Commun. Math. Phys.* **31** (1973) 259.
57. T. W. B. Kibble and G. E. Volovik, *Pis'ma Zh. Éksp. Teor. Fiz.* **65** (1997) 96 [JETP

Lett. **65** (1997) 102].

58. G. E. Volovik, Physica B **280** (2000) 122.
59. T. W. B. Kibble, Phys. Rept. **67** (1980) 183.
60. W. H. Zurek, Acta Phys. Polon. B **24** (1993) 1301.
61. P. Laguna and W. H. Zurek, Phys. Rev. D **58** (1998) 085021 [hep-ph/9711411].
62. A. Yates and W. H. Zurek, Phys. Rev. Lett. **80** (1998) 5477 [hep-ph/9801223].
63. G. J. Stempfens, L. M. A. Bettencourt and W. H. Surek, cond-mat/0108127.
64. W. H. Zurek, Phys. Rept. **276** (1996) 177 [cond-mat/9607135].
65. M. Hindmarsh and A. Rajantie, hep-ph/0103311.
66. A. Rajantie, J. Low. Temp. Phys. **124** (2001) 5 [cond-mat/0102403].
67. S. Digal, R. Ray and A. M. Srivastava, Phys. Rev. Lett. **83** (1999) 5030. [hep-ph/9805502].
68. A. J. Gill and R. J. Rivers, Phys. Rev. D **51** (1995) 6949 [hep-th/9410159].
69. F. C. Lombardo, F. D. Mazzitelli and R. J. Rivers, hep-ph/0102152.
70. B. Halperin, in *Physics of Defects*, edited by R. Balian, M. Kleman, and J. P. Poirier (North-Holland, New York, 1981).
71. F. Liu and G. F. Mazenko, Phys. Rev. B **46** (1992) 5963.
72. G. Karra and R. J. Rivers, hep-ph/9603413.
73. G. Karra and R. J. Rivers, Phys. Lett. B **414** (1997) 28 [hep-ph/9705243].
74. G. Karra and R. J. Rivers, Phys. Rev. Lett. **81** (1998) 3707 [hep-ph/9804206].
75. G. D. Lythe, Phys. Rev. E **53** (1996) R4271.
76. E. Moro and G. Lythe, Phys. Rev. E **59** (1999) R1303.
77. J. Dziarmaga, Phys. Rev. Lett. **81** (1998) 1551.
78. J. M. Cornwall, R. Jackiw and E. Tomboulis, Phys. Rev. D **10** (1974) 2428.
79. E. Calzetta and B. L. Hu, Phys. Rev. D **37** (1988) 2878.
80. S. Chang, Phys. Rev. D **12** (1975) 1071.
81. D. Boyanovsky, D. Lee and A. Singh, Phys. Rev. D **48** (1993) 800 [hep-th/9212083].
82. N. D. Antunes and L. M. Bettencourt, Phys. Rev. D **55** (1997) 925 [hep-ph/9605277].
83. M. Bowick and A. Momen, Phys. Rev. D **58** (1998) 085014 [hep-ph/9803284].
84. G. J. Stephens, E. A. Calzetta, B. L. Hu and S. A. Ramsey, Phys. Rev. D **59** (1999) 045009 [gr-qc/9808059].
85. J. Berges and J. Cox, hep-ph/0006160.
86. G. Aarts and J. Berges, hep-ph/0103049.
87. G. J. Cheetham and E. J. Copeland, Phys. Rev. D **53** (1996) 4125 [gr-qc/9503043].
88. S. P. Kim and F. C. Khanna, hep-ph/0011115.
89. M. Salle, J. Smit and J. C. Vink, Phys. Rev. D **64** (2001) 025016 [hep-ph/0012346].
90. D. Y. Grigoriev and V. A. Rubakov, Nucl. Phys. B **299** (1988) 67.
91. I. Montvay and G. Münster, *Quantum Fields of a Lattice* (Cambridge University Press, Cambridge, 1997).
92. H. J. Rothe, *Lattice Gauge Theories: an Introduction* (World Scientific, Singapore, 1998).
93. G. Parisi and Y. Wu, Sci. Sin. **24** (1981) 483.
94. A. Ukawa and M. Fukugita, Phys. Rev. Lett. **55** (1985) 1854.
95. N. Metropolis, A. W. Rosenbluth, M. N. Rosenbluth, A. H. Teller and E. Teller, J. Chem. Phys. **21** (1953) 1087.
96. M. Creutz, Phys. Rev. D **21** (1980) 2308.
97. S. Duane, A. D. Kennedy, B. J. Pendleton and D. Roweth, Phys. Lett. B **195** (1987) 216.
98. M. Laine, Nucl. Phys. B **451** (1995) 484 [hep-lat/9504001].
99. M. Laine and A. Rajantie, Nucl. Phys. B **513** (1998) 471 [hep-lat/9705003].
100. D. Bodeker, L. McLerran and A. Smilga, Phys. Rev. D **52** (1995) 4675 [hep-th/9504123].

101. G. D. Moore and K. Rummukainen, Phys. Rev. D **61** (2000) 105008 [hep-ph/9906259].
102. P. Laguna and W. H. Zurek, Phys. Rev. Lett. **78** (1997) 2519 [gr-qc/9607041].
103. P. Laguna and W. H. Zurek, cond-mat/9705141.
104. N. D. Antunes, L. M. Bettencourt and W. H. Zurek, Phys. Rev. Lett. **82** (1999) 2824 [hep-ph/9811426].
105. L. M. Bettencourt, N. D. Antunes and W. H. Zurek, Phys. Rev. D **62** (2000) 065005 [hep-ph/0001205].
106. G. J. Stephens, Phys. Rev. D **61** (2000) 085002 [hep-ph/9911247].
107. J. Ambjorn and A. Krasnitz, Phys. Lett. B **362** (1995) 97 [hep-ph/9508202].
108. K. J. Moriarty, E. Myers and C. Rebbi, Phys. Lett. B **207** (1988) 411.
109. K. Kajantie, M. Karjalainen, M. Laine, J. Peisa and A. Rajantie, Phys. Lett. B **428** (1998) 334 [hep-ph/9803367].
110. J. Ranft, J. Kripfganz and G. Ranft, Phys. Rev. D **28** (1983) 360.
111. D. Ibaceta and E. Calzetta, Phys. Rev. E**60** (1999) 2999 [hep-ph/9810301].
112. J. Dziarmaga, P. Laguna and W. H. Zurek, cond-mat/9810396.
113. I. S. Aranson, N. B. Kopnin and V. M. Vinokur, Phys. Rev. Lett. **83** (1999) 2600.
114. I. S. Aranson, N. B. Kopnin and V. M. Vinokur, Phys. Rev. B **63** (2001) 184501.
115. R. D. Pisarski, Phys. Rev. Lett. **63** (1989) 1129.
116. U. Kraemmer, A. K. Rebhan and H. Schulz, Annals Phys. **238**, 286 (1995) [hep-ph/9403301].
117. B. J. Nauta, Nucl. Phys. B **575** (2000) 383 [hep-ph/9906389].
118. A. Rajantie and M. Hindmarsh, Phys. Rev. D **60** (1999) 096001 [hep-ph/9904270].
119. G. D. Moore, C. Hu and B. Muller, Phys. Rev. D **58** (1998) 045001 [hep-ph/9710436].
120. J. Blaizot and E. Iancu, Nucl. Phys. B **557** (1999) 183 [hep-ph/9903389].
121. D. Bodeker, G. D. Moore and K. Rummukainen, Phys. Rev. D **61** (2000) 056003 [hep-ph/9907545].
122. S. Ducci, P. L. Ramazza, W. Gonzalez-Vinas and F. T. Arecchi, Phys. Rev. Lett. **83** (1999) 5210.
123. S. Casado, W. Gonzalez-Vias, H. Mancini and S. Boccaletti, Phys. Rev. E **63** (2001) 057301.
124. J. R. Anglin and W. H. Zurek, Phys. Rev. Lett. **83** (1999) 1707 [quant-ph/9804035].
125. R. Carmi and E. Polturak, Phys. Rev. B **60** (1999) 7595.
126. R. Carmi, E. Polturak and G. Koren, Phys. Rev. Lett. **84** (2000) 4966.
127. P. G. de Gennes and J. Prost, *The Physics of Liquid Crystals* (Clarendon, Oxford, 1993).
128. V. L. Ginzburg and L. P. Pitaevskii, Zh. Eksp. Teor. Fiz. **34** (1958) 1240 [Sov. Phys. JETP **7** (1958) 858].
129. A. J. Gill and T. W. B. Kibble, J. Phys. A **29** (1996) 4289.
130. M.E. Dodd *et al.*, J. Low Temp. Phys. **115** (1999) 89. [cond-mat/9810107].
131. G. E. Volovin and V. P. Mineev, Sov. Phys. JETP **45** (1977) 2256 [Zh. Eksp. Teor. Fiz. **72** (1977) 1186].
132. V. B. Eltsov, T. W. B. Kibble, M. Krusius, V. M. Ruutu and G. E. Volovik, Phys. Rev. Lett. **85** (2000) 4739 [cond-mat/0007369].
133. S. Rudaz, A. M. Srivastava and S. Varma, Int. J. Mod. Phys. A **14** (1999) 1591.
134. W. H. Zurek, L. M. Bettencourt, J. Dziarmaga and N. D. Antunes, Acta Phys. Polon. B **31** (2000) 2937.
135. S. J. Bending, Adv. Phys. **48** (1999) 449.
136. K. Harada *et al.*, Nature **360** (1992) 51.
137. P. E. Goa, H. Hauglin, M. Baziljevich, E. Il'yashenko, P. L. Gammel and T. H. Johansen, cond-mat/0104280.
138. V. V. Moshchalkov *et al.* Phys. Rev. B **57** (1998) 3615.

139. E. Kavoussanaki, R. Monaco and R. J. Rivers, Phys. Rev. Lett. **85** (2000) 3452 [cond-mat/0005145].